# 6

# Electronic and electro-optic molecular materials and devices

In Chapter 3 the electronic behaviour of inorganic semiconductors with reduced dimensionality was described. Here we consider the related, but more recent, field of organic electronics and optoelectronics, as well as the recent discovery carbon nanotubes. We shall also introduce organic devices in the present chapter, specifically field effect transistors, light-emitting diodes and photovoltaics. Although in this chapter we are primarily interested in the basic science behind organic electronics and optoelectronics, the knowledge gained will be used elsewhere in this volume, notably Section 8.8.1, for its application in nanotechnology.

## 6.1 CONCEPTS AND MATERIALS

### 6.1.1 The solid state: crystals and glasses

Organic matter often crystallizes only in part, or not at all. In particular, polymers often solidify in the form of a *glass*, but there are a number of low molecular weight organic materials that also form glasses, and there are inorganic glass formers as well; e.g., silicon oxide used for windows. Roughly speaking, a glass displays the mechanical properties of a solid (similar to crystalline solids), but the structure is disordered as in a liquid. In thermodynamic terms, the glassy state is a non-equilibrium state. However, particularly for polymeric glasses, the relaxation time to reach equilibrium can diverge to infinity at the Vogel–Fulcher temperature, well above absolute zero; thus the non-equilibrium state is no longer transient. Thermodynamic theories have been tailored to accommodate the permanent non-equilibrium nature of the glassy state, and to describe the *glass transition* above which the material regains its fluidity and reapproaches thermodynamic equilibrium. These are powerful theories, but currently no comprehensive

*Nanoscale Science and Technology* Edited by R. W. Kelsall, I. W. Hamley and M. Geoghegan

molecular theory of the glass transition based on first principles is available. The situation is similar to that in superconductivity at a time when the powerful, yet phenomenological Landau–Ginzburg (thermodynamic) theory was available, but not the microscopic Bardeen–Cooper–Shrieffer theory. The most important fact about the glassy state in the context of organic semiconductors is that the glass is structurally disordered like a liquid. Consequently, unlike crystalline materials there is no translation symmetry and Bloch's theorem (Section 1.2.6) does not apply.

For our context, the key difference between organic and inorganic solid matter is that excitations in inorganic matter are delocalized and best described by a wave vector $\mathbf{k}$, whereas in organic matter, excitations are localized and $k$ is not a good quantum number. To understand *organic semiconductors*, and maybe *synthetic metals*, we have to understand how something like a band gap can arise within a single molecule. The key to this understanding lies in the chemistry of carbon.

## 6.1.2 Chemistry of carbon

The most common carbon isotope is $^{12}C$ (the nucleus has six neutrons and six protons), but there is a natural abundance of 1.2% of the $^{13}C$ isotope with seven neutrons. This nucleus has a nuclear magnetic moment, which is used in NMR. In atomic carbon the six electrons occupy the orbitals in Table 6.1.

1s refers to the electronic state in which the principle quantum number (QN) is $n = 1$, the orbital QN is $l = 0$, and the magnetic QN is 0; there are two electrons occupying 1s due to their two spins. In a similar way, the 2s and 2p orbitals are filled with two electrons each. The electronic configuration is written as $1s^2 2s^2 2p^2$.

### 6.1.2.1 Hybrid orbitals

Carbon, like many chemical elements, forms covalent bonds. The driving force for chemical reaction is the desire to share electrons between different atoms to complete electronic shells. Thus, usually:

$$\text{atomic orbitals} \rightarrow \text{molecular orbitals.}$$

So C should form two bonds to add two electrons to complete the vacancies: one to $p_x$ and one to $p_y$. Carbon should be divalent – it should form two single bonds. But in reality it forms four bonds. In C, and some other atoms, chemical bonding proceeds via intermediate steps: *promotion* and *hybridization*:

$$\text{atomic orbitals} \rightarrow \text{hybrid orbitals} \rightarrow \text{molecular orbitals.}$$

**Table 6.1** Orbitals of carbon

| Orbital | 1s | 2s | $2p_x$ | $2p_y$ | $2p_z$ |
|---|---|---|---|---|---|
| Number of electrons | 2 | 2 | 1 | 1 | 0 |

For hybridization, C promotes one 2s electron into the empty $p_z$ orbital, so we arrive at $1s^2 2s^1 2p^3$. Then C combines (hybridizes) the remaining 2s electron and either:

three 2p orbitals $\rightarrow sp^3$ hybrids, or
two 2p orbitals $\rightarrow sp^2$ hybrids, or
one 2p orbital $\rightarrow$ sp hybrid.

$sp^3$ hybrid orbitals have four fingers pointing into the corners of a tetrahedron. The tetrahedral bond angle is 109.5°. In this form C can form four bonds by sharing electrons with hydrogen 1s shells (e.g., $CH_4$, methane) or with other $sp^3$ carbons (e.g., $H_3C{-}CH_3$, ethane). The C–C bond in ethane is called a $\sigma$ bond. $\sigma$ bonds are very strong; diamond entirely consists of carbon held together by $\sigma$ bonds.

$sp^2$ hybrid orbitals have three fingers in a plane, at angles of 120° to each other, plus one remaining p orbital perpendicular to the plane. This configuration is found in graphite, in which the $sp^2$ bonding results in sheets of hexagonally ordered carbon atoms (known as graphene sheets); the sheets are stacked one on top of the other, with the sheets only weakly bonded together. In this form C needs another $sp^2$ hybrid C to form a molecule; for example ethene ($H_2C{=}CH_2$) in which two of the three fingers of each C bond to H as before, and the third overlaps with another C $sp^2$ orbital to form a bond ($\sigma$ bond). The remaining p orbitals of either C overlap, as well, to form another carbon–carbon bond; the so-called $\pi$ bond. A $1\sigma + 1\pi$ bond constitutes a carbon double bond. This is a weaker bond, and the respective orbital is more *delocalized*; i.e., it occupies a relatively large space rather far away from its original carbon.

sp hybrid orbitals have two fingers along one axis (say the $x$ axis) at 180° to each other, plus two remaining p orbitals (along the $y$ and $z$ axes). In this form C can bond with two hydrogens and another sp hybrid. It forms one $\sigma$ bond between the sp orbitals, plus the remaining two p orbitals of each molecule overlap to form two $\pi$ bonds (a carbon triple bond): this is ethyne ($HC{\equiv}CH$), also called acetylene.

### 6.1.2.2 The benzene ring

A regular hexagon is a planar structure with six sides and six corners, each with internal angle of 120°. $sp^2$ hybrid orbitals have an angle of 120° with respect to each other. Hence by $\sigma$ bonding six $sp^2$ carbons, we can form a regular hexagon. Each carbon will form two $\sigma$ bonds, one with each of its neighbours. There remains one $sp^2$ orbital per carbon to be capped; e.g., by a hydrogen. The remaining p orbitals will again overlap to form $\pi$ bonds. The resulting structure may look like Figure 6.1.

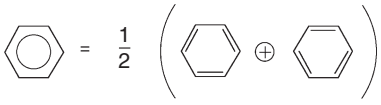

**Figure 6.1** The chemical structure of benzene can be seen to be a mixture of two possible 'borderline' structures

It is not quite clear where the $\pi$ bonds should be. In reality, an intermediate state is adopted, where the $\pi$ electrons are completely delocalized, so that it is impossible to assign double bonds (Figure 6.1). The $\pi$ electrons form a cloud that spans the entire molecule. The side of a ring is 1.39 Å in length, intermediate between the C–C and C=C bond lengths.

#### 6.1.2.3 Conjugated molecules

The benzene ring is the prototype of a *conjugated* molecule – a molecule with alternating single/double or single/triple carbon bonds. In conjugated molecules, $\pi$ electrons delocalize throughout the entire molecule and are relatively loosely bound. We have been thinking of conjugated molecules being built step by step, by binding hybridized carbons together in a *linear combination of atomic orbitals* (LCAO). In the *molecular orbitals* (MO) description (introduced in Section 1.2.2), we instead imagine a given, rigid set of points at which atomic nuclei are fixed, and fill that skeleton with electrons to arrive at the molecule. The LCAO and MO approaches correspond to two schools of quantum chemistry and computer simulation. Both approaches should lead to the same molecules, but in the MO picture, the correspondence to semiconductors is easier to see. We need $N$ electrons in the molecule to balance $N$ positive charges. The first electrons will cluster closely to the atomic nuclei, resulting in almost undisturbed atomic orbitals; this is equivalent to saying that the carbon 1s electrons, for example, do not participate in chemical bonds, but the last few electrons will enter what we have called delocalized $\pi$ orbitals. Although we can trace $\pi$ orbitals to the hybridized atomic orbitals of carbon, we have seen that in a conjugated molecule, they may delocalize far from their original carbon, hence for the $\pi$ cloud, the MO picture is more appealing.

The last pair of electrons (one for each spin state) to be filled into the molecule occupy a molecular orbital that is called the *highest occupied molecular orbital* (HOMO). Note that a half-filled HOMO would imply an unpaired spin; i.e., the molecule would be a *radical*. Since the completion of electronic shells is the driving force behind chemical reactions, radicals usually appear at intermediate stages of chemical reactions, but not as end product. The next molecular orbital beyond the HOMO is called the *lowest unoccupied molecular orbital* (LUMO). The HOMO and LUMO are collectively known as *frontier orbitals*.

Due to the delocalized and weakly bound character of $\pi$ electron clouds, conjugated molecules can be ionized relatively easily, and the electron vacancy or surplus electron can travel along the molecule with relative ease. This situation is reminiscent of the VB/CB description of inorganic semiconducting crystals. Due to this analogy, the energy difference between LUMO and HOMO in a conjugated molecule is called the *band gap*. However, we will soon address the limits of the analogy between inorganic and organic semiconductors.

#### 6.1.2.4 Buckminsterfullerene

Until 1990 it was universally thought that only two allotropes of carbon existed, diamond and graphite. The first evidence for the existence of an alternative form was the observation of enhanced absorption of stellar radiation, at a specific frequency

corresponding to the predicted optical response of a 60-atom carbon cluster. The cluster has the same topography as a common soccer ball, with 20 hexagonal faces and 5 pentagonal faces. Molecular dynamics simulations have shown that this is the most stable possible configuration for a closed carbon cluster. The $C_{60}$ molecule was originally christened buckminsterfullerene, after the architect Buckminster Fuller, who had designed a geodesic dome in the shape of a soccer ball. Subsequently, $C_{60}$ molecules have been nicknamed buckyballs, and the whole family of carbon clusters (70-, 76-, 80- and 84-atom clusters have also been discovered) are referred to as fullerenes. In the solid state, $C_{60}$ molecules assemble into a face-centred cubic lattice with a lattice constant of around 1 nm. Small atoms, such as potassium, can be introduced to interstitial sites in the lattice by heat treatment, and this changes the crystal from an insulating state to an electrically conducting state. Atoms can also be introduced inside the $C_{60}$ cages.

### 6.1.3 Examples of organic semiconductors

The appendix to this chapter comprises a list of important conjugated molecules and polymers in the field of organic semiconductors. The acronyms by which they are referred to in this book are also provided along with a brief discussion of their properties. Readers are encouraged to familiarize themselves with the variety of conjugated materials that have been explored.

Historically, the organic semiconductor discipline has distinguished between polymeric and low molecular weight organic semiconductors. This distinction is nowadays blurred due to the advent of a number of hybrid materials, which combine properties and attributes of low molecular weight and polymeric materials. A few examples of these are included in the appendix.

The sheer length of the appendix – which is still incomplete – underscores one of the key assets of organic semiconductors: the practically unlimited diversity of synthetic organic chemistry allows the tailoring of materials with a large portfolio of properties. Besides this variety, it should be remembered that materials which are nominally the same often show very different performance in devices. Device performance can be very sensitive to low levels of impurities and/or chemical defects, and different chemical routes that lead to the same material often introduce different levels and types of defects and/or impurities. Even if the chemistry is ideal, the same material can still display very different properties when processed in different ways. The solvent and casting method used for solution processing, or deposition rate, type and temperature of substrate for evaporated films, thermal treatment cycles, and the presence or absence of even trace amounts of oxygen can have a decisive impact on the resulting device.

### 6.1.4 Excitations in organic semiconductors

In any semiconductor application, the material will not be in its ground state. To transport charge and/or emit light, the semiconductor needs to sustain excitations, and in the case of charge transport, these excitations also need to be mobile. In this section the

fundamental properties of these excitations are discussed, whilst in Section 6.1.5, the generation and migration of excitations is described.

### 6.1.4.1 Polarons and excitons

When an electron is taken away from the HOMO or added to the LUMO of a molecule, the resulting molecule is termed a *radical ion*; namely a radical cation for positive charge, and radical anion for negative charge. The word 'radical' refers to the net spin the molecule will have due to the unpaired remaining (or added) electron. After removal or addition of the electron, molecular orbitals and the positions of nuclei will respond by a relaxation to a new position of minimum energy. Radical ions are often called *polarons*, analogous to the term used for inorganic semiconductors. Again, however, the inorganic polaron is delocalized with an associated wavevector **k** describing its coherent movement; the radical ion is not delocalized.

Due to the localized character of the polaron, its charge strongly couples to molecular geometry. Bond distances and angles will be distorted compared to the neutral molecule. This distortion will always reduce the energetic cost of forming a polaron. Therefore removing an electron costs somewhat less energy than the HOMO suggests, and an electron joining the molecule gains somewhat more energy than the LUMO suggests, because HOMO/LUMO levels are calculated for undistorted molecular geometries. Instead, the energies required for polaron formation are called the ionization potential $I_p$, and electron affinity $E_a$, respectively (we define these two parameters in Figure 6.7). As a practically important example, a neutral and a positively charged polythiophene segment are sketched in Figure 6.2. Note how the missing electron, or *hole*, leads to a redistribution of the $\pi$-bonds and hence to different nuclear distances and positions.

When an electron is removed from the HOMO but is placed into the LUMO instead of being removed entirely from the molecule, we arrive at an electrically neutral excitation, the so-called *exciton*. A typical way of lifting an electron from the HOMO into the LUMO is via the absorption of a photon. The $\pi$ electrons redistribute into the excited $\pi^*$ orbitals, which are also known as antibonding orbitals, as they destabilize the molecule. Nevertheless, the strong $\sigma$ bonds are crucial in keeping the molecule intact. Again, the excitation leads to a related relaxation of the surrounding crystal lattice or molecule. Figure 6.3 shows the geometric relaxation and redistribution of electron density in an excited phenylene–vinylene segment.

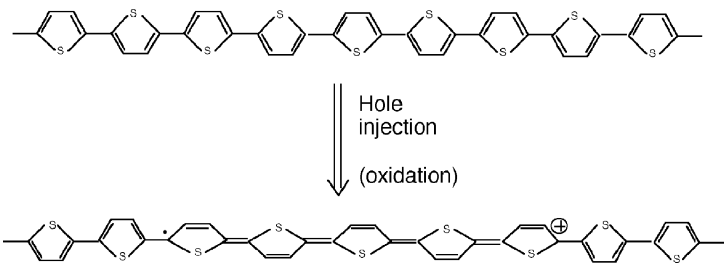


**Figure 6.2** A polythiophene segment and the derived radical cation

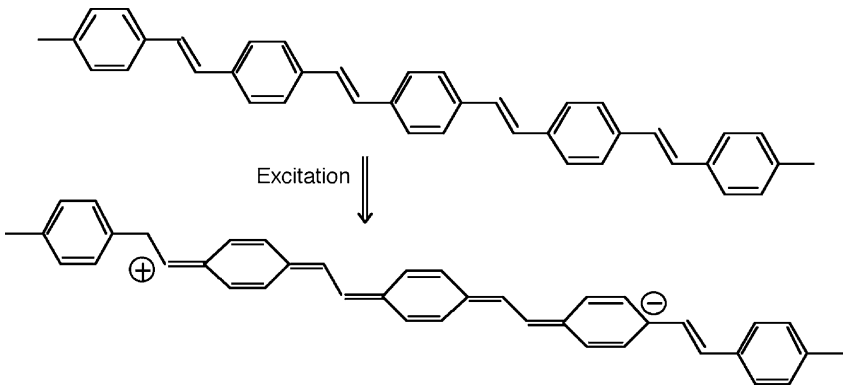


**Figure 6.3** The transition from an aromatic, 'bonding' $\pi$ phenylene–vinylene system to a quinoidal, 'antibonding' $\pi^*$ system on optical or electrical excitation

The size of the exciton is about three repeat units, or 10 nm, and the exciton has clearly intramolecular, one-dimensional character. This makes organic excitons *Frenkel* excitons. Typical exciton binding energies $E_b$ are in the range 0.2–0.5 eV. Note how considerable ambiguity arises in the term 'band gap', which can mean either the energy difference between LUMO and HOMO, or $I_p - E_a$ or $(I_p - E_a) - E_b$.

Figure 6.4 is an alternative, more schematic, representation of the electronic ground state, radical ions (here called polarons), and excitons in organic semiconductors. It shows two different types of exciton: *singlet* and *triplet* excitons. There are three ways in which hole and electron spin can combine so that the resulting overall spin part of the wavefunction is symmetric under particle exchange, and has total spin $S = 1$, namely $|\uparrow\uparrow\rangle, |\downarrow\downarrow\rangle$, and $(1/\sqrt{2})(|\uparrow\downarrow\rangle + |\downarrow\uparrow\rangle)$. Excitons with that property are called triplet excitons. The combination of spins $(1/\sqrt{2})(|\uparrow\downarrow\rangle - |\downarrow\uparrow\rangle)$ results in a spin part of the wavefunction that is antisymmetric under particle exchange, and total spin $S = 0$. This combination is called a singlet exciton.

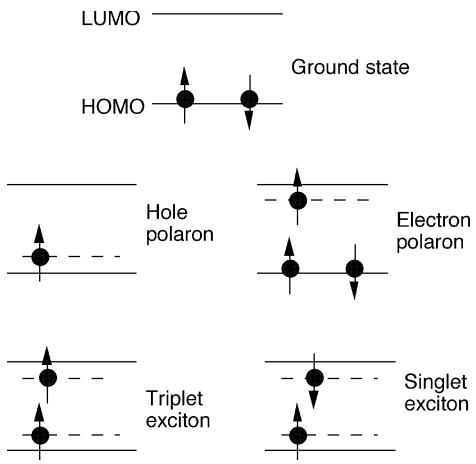


**Figure 6.4** Energy level diagrams for excitations in organic semiconductors

### 6.1.4.2 Light emission from organic molecules

In simplified terms, the absorption of a photon that has generated an exciton on an organic molecule can in some cases be reversed (ignoring some intermediate steps discussed below). The excited electron drops back from the LUMO into the HOMO, emitting a photon in the process. This phenomenon is known as *fluorescence*. Since excitons can also be generated electrically by combination of polarons, this paves the way to organic electroluminescence (EL). First, we shall discuss fluorescence in some detail, using a framework based on ground- and excited-state molecular orbitals. Then we shall return to discuss a striking difference between fluorescence and EL, which is best understood using the more schematic picture of Figure 6.4.

*Fluorescence in the MO picture*

Figure 6.5 presents a schematic view of fluorescence in the MO picture. The two curves in the potential energy–distance diagram describe the ground state ($S_0$) and the first excited state ($S_1$) of a chemical bond; the equilibrium distance is the bond length, which is longer for the excited state. The horizontal lines represent the vibrational states of the bonds; i.e., nuclear distance oscillates around the equilibrium bond length within the limits of the intersection of the horizontal line with the potential curve.

The difference between vibrational levels is the vibrational-electronic or *vibronic spacing*, of order 0.1 eV (~1100 K). Consequently, at room temperature, almost all bonds are in the lowest vibronic level of the ground state. From there they may be lifted into the first excited state by absorption of a photon. This process is governed by the *Franck–Condon principle*, which states that electronic transitions are much faster than nuclear rearrangement. Hence transitions occur vertically in the diagram, from ground state equilibrium position to the most probable interatomic spacing of a

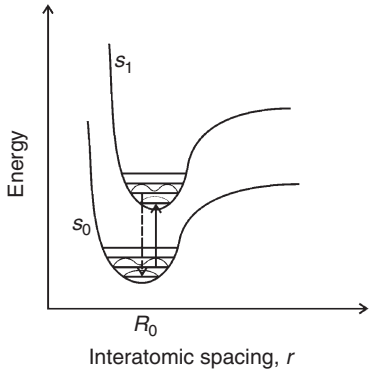


**Figure 6.5** Energy diagram for molecules in ground ($S_0$) and excited ($S_1$) electronic states. An absorption transition and an emission transition between these levels are shown for the first two vibronic states. These transitions occur to minimize any change in interatomic spacing, and this can only rapidly occur when the 'probability' of a given spacing is large in both the initial and final levels. Example probability functions are shown in the figure. Note that the interatomic spacing $r$ is equal to the equilibrium spacing $R_0$ only in the ground vibronic state of the ground electronic state

vibrational mode of the excited state that is close to the ground state equilibrium distance (Figure 6.5). The relative intensity of these is controlled by the overlap integral between the electronic ground state and the vibronic ground state (0 vibronic state) and excited state and vibronic state $0, 1, 2, \ldots$ (Franck–Condon factors). In the excited state, however, there will be a rapid radiationless relaxation (typically of order $10^{-12}$ s) of the excited state into its lowest vibronic level (internal conversion). From there the photon may be re-emitted after typically between 1 and 10 ns with a transition to the lowest vibronic level of the ground state (0–0 transition), the first vibrational state (0–1 transition), second vibrational state (0–2 transition), and so on. This gives rise to the occurrence of several peaks in the absorption and fluorescence spectra, the so-called vibronic structure or *vibronic satellites*. Vibronic spacing is similar in the ground and excited states, so they often appear like mirror images (Figure 6.6). The onset of absorption or the intersection of the absorption and photoluminescence (PL) spectra in a plot such as Figure 6.6 is often called the *optical band gap*.

The *photoluminescence quantum yield* $\eta_{\mathrm{PL}}$ is defined as the ratio of the number of photons in to the number of photons out. Fluorescent decays of an excited state back to the ground state compete with a number of non-radiative decay processes (fluorescence quenching). The fluorescence quantum yield can be expressed as the result of a competition between fluorescent processes with rate $\Gamma$ and non-fluorescent processes with rate $k_{\mathrm{n}}$:

$$\eta_{\mathrm{PL}} = \frac{\Gamma}{\Gamma + k_{\mathrm{n}}}. \tag{6.1}$$

In a good dye this should be as high as possible. Perylene has $\eta_{\mathrm{PL}} = 0.94$ in cyclohexane solution, and many modern conjugated polymers exceed a 50% quantum yield even in the solid state. However, some conjugated polymers display rather low fluorescence quantum yields. PATs, for example, have rather moderate quantum yields and are used widely in non-emissive transistors, but not in light emitting devices (see the Appendix for the chemical formula of PAT). This is because they display a molecular dipole moment that enhances non-radiative decay channels.

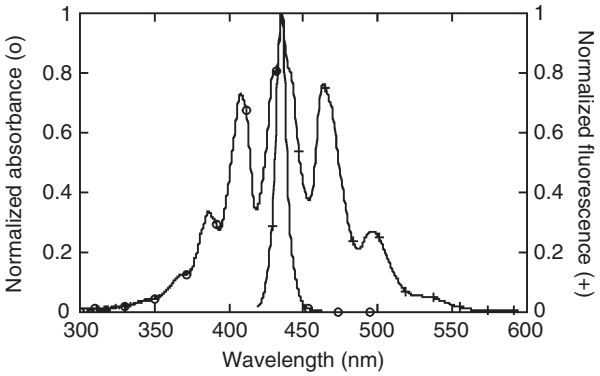


**Figure 6.6** Absorption and emission spectra of perylene. Data from http://omlc.ogi.edu/spectra/PhotochemCAD/html

*Fluorescence, parity, electroluminescence and phosphorescence*

The observation that poly(arylene vinylene)s or poly(arylene)s such as PPV, PPE, PF, PPP and MeLPPP do display bright fluorescence, whereas PATs have somewhat lower quantum yields, can be understood through the different strength of non-radiative decay channels. However, polyenes such as PA and PDA display $\eta_{PL} \approx 0$, without strong molecular dipoles. A different mechanism must be at work that forbids fluorescence in the polyenes.

A necessary condition for a molecule to be fluorescent is *parity alternation* between the ground state and the lowest-lying excited state. The simplest quantum mechanical model of bound electrons is a single electron bound to a harmonic potential (a harmonic oscillator). The harmonic oscillator has discrete energy eigenstates that can be labelled by a quantum number $n$. For all odd-numbered eigenstates of the harmonic oscillator, including the ground state $n = 1$, eigenstates obey $\Psi_n(-x) = \Psi_n(x)$; i.e., the state is said to have *even* ($g$) parity. For even-numbered eigenstates, including the lowest-lying excited state $n = 2$, eigenstates obey $\Psi_n(-x) = -\Psi_n(x)$; i.e., the state is said to have *odd* ($u$) parity. This property is called parity alternation.

A molecule is rather different from a harmonic oscillator. Nevertheless, molecular orbitals do display either $g$ or $u$ parity as well. However, parity alternation may be broken, mainly because of strong electron–electron interactions. Note the harmonic oscillator Hamiltonian contains no such interactions.

Fluorescent transitions can take place only between states of different parity. This is called a *selection rule*, and is related to the fact that a photon carries unit angular momentum $\hbar$ needs to be supplied from the emitting molecule. Only in molecules that retain parity alternation between ground and first excited state can we observe fluorescence. Experience (as well as extensive quantum chemical computations) shows that the strong electron–electron interactions in the polyenes break parity alternation and are therefore not fluorescent. In polyarylenes and polyarylenevinylenes, however, parity alternation is preserved.

In light-emitting devices, light is generated not by the absorption of a photon, but by the combination of an electron and a hole polaron. Figure 6.4 clearly shows that an electron in the LUMO and an electron vacancy (hole) in the LUMO can combine to form an exciton. The fluorescence emitted from an electrically generated exciton is called *electroluminescence* (EL). However, there is a fundamental difference between the formation of excitons by absorption of light and by combination of polarons. The ground state of a molecule carries net spin $S = 0$, and is thus a singlet state. The angular momentum $\hbar$ of a photon interacts with the orbital angular momentum of the molecular wavefunction (this leads to the parity alternation selection rule). However, to a first approximation, photon angular momentum does not interact with spin angular momentum, and thus cannot flip electron spins. Therefore absorption of a photon can only generate singlet excitons. Conversely, only singlet excitons have a *dipole-allowed* transition to the molecular ground state; fluorescence links an excited singlet state to the singlet ground state.

On electrical generation, however, polarons can combine to form triplet as well as singlet excitons. In fact, there are three combinations leading to a triplet, and only one leading to a singlet. If polaron–polaron capture were independent of mutual spin orientation (as one naively expects), only one in four electrically generated excitons would be able

to yield electroluminescence: $\eta_{EL} = \eta_{PL}/4$. This limits the efficiency of EL devices, and has been subject to extensive applied and fundamental research (Section 6.2.3).

In some cases, light can be emitted from triplet excitons, although that transition is dipole-forbidden. This is facilitated by so-called *spin–orbit coupling*, which results from the fact that both spin and orbital angular momentum imply a magnetic moment, which interact via a product term $\mathbf{L} \cdot \mathbf{S}$ in the molecular Hamiltonian. In effect, the angular momentum $\hbar$ required for emission of a photon can be provided from the triplet spin, instead of orbital angular momentum. Remember that $S = 1$ for a triplet, thus the transition from a triplet to a singlet releases unit angular momentum $\hbar$. To facilitate spin–orbit coupling, atoms are required with electrons in states with high orbital angular momentum $\mathbf{L}$, as this strengthens the $\mathbf{L} \cdot \mathbf{S}$ term. Generally, these are relatively heavy atoms (heavier than carbon) that have higher atomic shells occupied, such as sulphur and phosphorus. The resulting dipole-forbidden emission is called *phosphorescence*. The rate of a dipole-forbidden transition is much lower than for a dipole-allowed transition. Typical phosphorescence lifetimes can be up to $\sim$1 ms.

#### 6.1.4.3 Controlling the band gap

The wavelength of light emitted from an excited molecule, and therefore the colour of emission, is determined by the band gap. In particular, for light emission applications it is paramount to control the band gap. One of the key assets of organic semiconductors is that the band gap can be fine-tuned by synthetic chemistry. In fact, $E_a$ and $I_p$ can often be manipulated rather independently of each other. This subject cannot be discussed systematically here, and the reader is referred to the review by Kraft and colleagues listed in the bibliography. Instead, the key concepts are illustrated by some examples.

The band gap of PATs and PDAs can be tuned rather widely by the attachment of *side chains*. We will see in Section 6.1.6.2 that side chains are essential to promote polymer solubility. Side chains lead to twisting of adjacent ring systems out of the coplanar conformation. The twist angle depends on the length, type and bulkiness of the side chains. The larger the twist, the poorer the overlap between $\pi$ systems, thus the larger the band gap becomes; a *blueshift* occurs. PATs and PDAs are the outstanding examples for *steric* band gap tuning. Another approach to blueshifting a band gap is to reduce $\pi$ coherence by deliberately introducing meta- instead of para-linked phenyl rings into the main chain of phenylene vinylenes.

When alkoxy rather than alkyl chains are attached to a ring system, the respective polymer ends up with a reduced band gap due to the influence the oxygen has on the benzene $\pi$ orbitals. This explains the reduced band gap in MEH-PPV as compared to PPV. A much stronger influence on the band gap is exercised by attaching strongly electron-withdrawing cyano groups to the vinylene bonds in phenylene vinylene. The resulting CN-PPV has a higher electron affinity than PPV or MEH-PPV. The band gap is reduced to give a red-emitting polymer, and the character of CN-PPV is changed to electron transporting, as compared to hole-transporting PPV. These are examples of *electronic* band gap tuning.

The side chains of polyfluorenes are not directly attached to the $\pi$ system, and thus can exercise only very little influence on the band gap. Band gap tuning is achieved by

*copolymerization* instead. Alternating copolymers of fluorene with two thiophene units (F8T2), or of fluorene with a bisthiadiazole unit (F8BT), both have a similar band gap in the green, compared to the blue band gap of the polyfluorene homopolymer. However, in F8T2 the reduction in band gap results from a reduced ionization potential, whereas in F8BT it results from a higher electron affinity.

## 6.1.5 Charge carrier injection and transport

The injection and transport of charge carriers is an issue of practical importance for semiconductor devices: Transistors require the injection of one type of carrier from an electrode, and rather fast mobility of that carrier. Light-emitting devices require the injection of carriers of both types from different electrodes. Photovoltaic devices need to separate excitons and transport the resulting carriers to opposite electrodes. It is thus paramount that we discuss the factors controlling carrier injection and transport.

### 6.1.5.1 Charge carrier injection

The characteristics of carrier injection from a metal electrode into a semiconductor are controlled by the work function $\Phi$ of the metal relative to the electron affinity $E_a$ of the semiconductor for electron injection, and relative to the ionization potential $I_p$ of the semiconductor for hole injection. An energy level diagram such as Figure 6.7 is often used

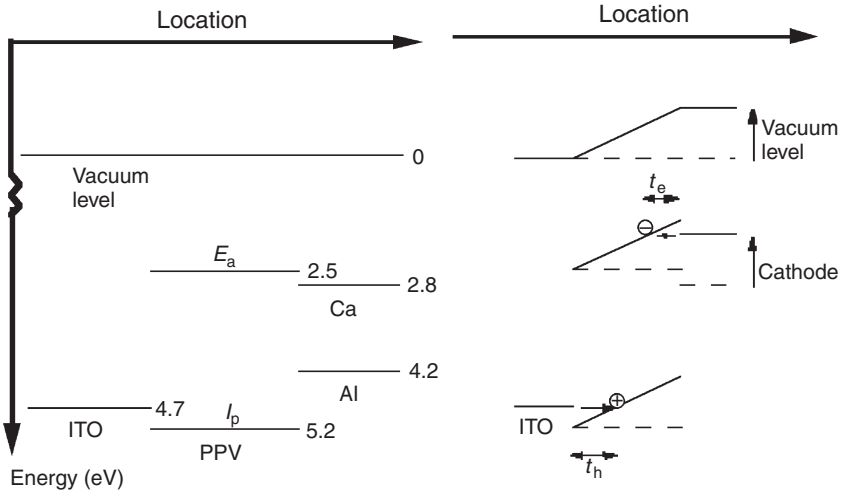


**Figure 6.7** Energy levels for a PPV layer sandwiched between unlike electrodes. Indium tin oxide (ITO) is a transparent metallic material that is commonly used as anode for OLEDs; the anodes are typically metals such as aluminium or calcium. Left: no bias voltage applied (numbers indicate associated energies relative to the vacuum level in eV). Right: a voltage is applied in forward bias. $t_e$ and $t_h$ are the respective distances that electrons and holes have to tunnel to be injected into the semiconductor. Note that under this bias, the vacuum level of the cathode moves relative to the anode

to illustrate carrier injection into an *organic light-emitting device* (OLED). Note that due to the molecular nature of organic semiconductors, there are no surface dangling bonds that can distort bulk energy levels. Also, organic semiconductors are generally not deliberately doped. Hence there is no band bending that could distort the level diagram.

The left-hand part of Figure 6.7, shows an *injection barrier* of 0.5 eV for holes from ITO into PPV, and 0.3 or 1.7 eV for electron injection from Ca or Al into PPV, respectively. For electron injection from ITO there would be a large barrier of 2.2 eV. Thus, the use of electrodes made from unlike metals defines a *forward* and *reverse bias* for the OLED. To minimize barriers, a high work function anode and a low work function cathode are required. However, for barriers of 0.5 eV, as shown here, the current density in a device under forward bias will be controlled by the injection of carriers across the barrier, rather than by the transport of carriers across a device.

The right-hand part of Figure 6.7 shows the same device (assuming a Ca cathode) under a forward bias. Carriers can now overcome injection barriers by tunnelling or by thermionic injection. The tunnelling current density $j$ ($j = I/A$ with current $I$, area $A$) against the applied voltage characteristic $j(V_{\text{bias}})$ is described by *Fowler–Nordheim (FN) tunnelling* and satisfies the following equation:

$$j_{\text{FN}} = \frac{C}{\Delta V}\left(\frac{V_{\text{bias}}}{d}\right)^2 \exp\left(-B\frac{d\,\Delta V^{3/2}}{V_{\text{bias}}}\right), \tag{6.2}$$

where $B$ and $C$ are constants, and $\Delta V$ is the injection barrier. Note that $j_{\text{FN}}$ depends on applied voltage $V_{\text{bias}}$ and film thickness $d$ only in the combination $V_{\text{bias}}/d$ such that $j_{\text{FN}}$ scales with the applied field $E$. Thermionic injection is described by the *Richardson–Schottky* equation:

$$j_{\text{RS}} = AT^2 \exp\left(\frac{-(\Delta V - V_{\text{m}}(E))}{k_{\text{B}}T}\right), \tag{6.3}$$

where $A$ is a constant and $V_{\text{m}}(E)$ describes the field-dependent lowering of the injection barrier by the attraction of the injected carrier to its mirror charge; $V_{\text{m}}(E) = \sqrt{eE/4\pi\varepsilon_{\text{r}}\varepsilon_0}$.

Generally, RS injection will dominate at low fields, and FN tunnelling at large fields. Experimental $j(V)$ results on MEH-PPV diodes can qualitatively be described by Equation (6.2), however, the absolute current density is several orders of magnitude lower than described by Equation (6.2). This is due to a large backflow of carriers from the semiconductor into the metal.

In the case $\Delta V \to 0$; i.e., when a work function is matched to the respective semiconductor level, the FN equation predicts a divergence of current density. Then the current density will be controlled by carrier transport across the film, rather than by injection, and the metal–semiconductor contact is termed *ohmic*. Practically, a contact can be considered ohmic whenever carrier transport is a more restrictive limit on current density than carrier injection. Roughly, barriers of 0.3 eV at the very most can be considered ohmic.

Ohmic contacts are generally desirable, and considerable effort has been devoted to increase the work function of the transparent ITO anode by a variety of physicochemical

treatment cycles. For example, recently it has become common to coat ITO with a thin film of the high work function synthetic metal PEDOT/PSS ($\Phi = 5.2\,\text{eV}$). The cathodes are commonly low work function materials such as Ca. These materials require protection from the ambient atmosphere, otherwise they would degrade rapidly. This can be provided by encapsulation or by capping with a more stable metal such as aluminium.

#### 6.1.5.2 Charge carrier transport: mobility

After injection, charge carriers in a semiconductor will generally move in the direction of the applied field (at least on average). Two types of motion are common: coherent (band-like) motion, described by a wavevector **k**, and incoherent (hopping-type) motion. In disordered materials with localized excitations, such as organic semiconductors, incoherent motion will prevail. This can be visualized as the superposition of a thermally driven random diffusion and a directed motion in the direction of the electric field. The first of these motions will not be considered here, as it is undirected and does not result in a net current when averaged over time or the ensemble. As a starting point, we shall consider the directed motion of charge carriers under an applied field in a fashion similar to the motion of a solid sphere in a viscous medium under the influence of a constant force (e.g., gravity). The sphere (or the carrier) will rapidly accelerate up to a steady-state velocity $v$, at which the friction exerted by the viscous medium balances the constant force. This velocity is given by

$$v = \mu E, \tag{6.4}$$

where $E$ is the electrical field, $E = V_{\text{bias}}/d$, and $\mu$ is the charge carrier mobility, typically quoted in units $\text{cm}^2\text{V}^{-1}\text{s}^{-1}$. Besides $I_\text{p}$ and $E_\text{a}$, the carrier mobility is one of the most important characteristics of an organic semiconductor, and can span a wide range of orders of magnitude, from around $10^{-7}$ to $10^{-1}\,\text{cm}^2\text{V}^{-1}\text{s}^{-1}$, within the regime of hopping-type transport. Considerably higher mobilities of up to $10^2\,\text{cm}^2\text{V}^{-1}\text{s}^{-1}$ or more can be observed for coherent motion in organic single crystals. However, applications based on organic single crystals are uncommon and will not be discussed here.

We also note that the analogy to the sphere in a viscous fluid cannot be pushed too far: it is deceptive to assume $v \propto E$ from the apparently simple Equation (6.4) as $\mu$ is a function of field $E$. Bässler in Marburg has carried out extensive computer simulations of hopping-type transport. In his model, he assumes that HOMO levels are not all equal in energy, but display a Gaussian distribution around the average HOMO. This energetic distribution is termed *diagonal disorder* and is characterized by a variance $\sigma^2$, or the dimensionless quantity $\hat{\sigma} = \sigma/k_\text{B}T$. The hopping rate is also affected by positional or *off-diagonal disorder* that is quantified by another variance, $\Sigma^2$. Bässler proposed the following $\Sigma$-dependent equation for $\mu$:

$$\mu(E,T) = \mu_0 \exp\left(-\left(\frac{2\hat{\sigma}}{3}\right)\right) \begin{cases} \exp\left(\left(\hat{\sigma}^2 - \Sigma^2\right)\sqrt{E}\right) & \text{for } \Sigma < 1.5 \\ \exp\left(\left(\hat{\sigma}^2 - 2.25\right)\sqrt{E}\right) & \text{for } \Sigma \geq 1.5 \end{cases} \tag{6.5}$$

### 6.1.5.3 Charge carrier transport: space charges

The current density $j$ that results from the drift of carriers in an applied field should be given as

$$j = qn\mu E = \sigma E \tag{6.6}$$

where $q = \pm e$ is the charge per carrier, $n$ is the carrier density, and $\sigma = qn\mu$ is the conductivity. Equation (6.6) is equivalent to Ohm's law with resistance $R = d/\sigma A$.

However, Equation (6.6) assumes that the electric field $E$ acting on each carrier at any position within the film is equal to the externally applied field. That will be true for low current densities, when the total charge of all carriers within the film at any one time, $Q_{\text{tot}}$, can be neglected with respect to the capacitance charge, $Q_{\text{cap}}$, of the film. $Q_{\text{cap}}$ is the charge the electrode/film/electrode structure can hold at the respective applied voltage as a capacitor, and $Q_{\text{tot}} \ll Q_{\text{cap}} = CV$, with $C = \varepsilon_0\varepsilon_{\text{r}}A/d$; thus $Q_{\text{tot}}/A \ll \varepsilon_0\varepsilon_{\text{r}}E$. When $Q_{\text{tot}}$ becomes comparable to $Q_{\text{cap}}$, the externally applied field becomes screened inside the film by *space charge*, and the local field acting on a carrier will be less than the applied field and will depend on position. To estimate the *space charge limited current* (SCLC) in that situation, we assume that we have charge/area, $Q_{\text{cap}}/A$, crossing the film per unit *transit time* $\tau$. $\tau$ is the time a carrier would require to cross the film in the space charge free limit, $\tau = d/\mu E$. This leads to an estimate of space charge limited current density $j_{\text{SCLC}} \approx Q_{\text{cap}}/A\tau = \varepsilon_0\varepsilon_{\text{r}}\mu V^2/d^3$.

The precise treatment of the current density in a semiconductor in the SCLC regime solves the relevant electromagnetic equations in a self-consistent manner, balancing the two competing effects of field screening by space charges and dispersal of space charges by field. This calculation leads to the following results:

$$E(x) = -\frac{3}{2}V\sqrt{\frac{x}{d^3}}, \tag{6.7a}$$

$$n(x) = \frac{3\varepsilon_{\text{r}}\varepsilon_0 V}{4\sqrt{xd^3}}, \tag{6.7b}$$

$$j_{\text{SCLC}} = \frac{9}{8}q\varepsilon_{\text{r}}\varepsilon_0\mu\frac{V^2}{d^3}, \tag{6.7c}$$

where $x$ is a spatial coordinate, electrodes are at $x = 0$ and $x = d$, and $E(x)$ and $n(x)$ are the position-dependent field and carrier density, respectively. Equation (6.7c) is known as *Child's law*. Note that $j \propto E(x)n(x)$ does *not* depend on $x$. The derivation of Equation (6.7) assumes mobility to be independent of $E$, and it cannot therefore be exactly correct for a Bässler-type $\mu(E)$ (Equation 6.5). Space charges screen the applied field in such a way that $E(0) = 0$; there is no field at the injecting electrode. Strictly, therefore, no current should be drawn across the electrode–semiconductor junction. Carrier diffusion, which we had ignored at the very beginning, comes to the rescue. However, we rely heavily on the assumption of an ohmic contact at the injecting electrode. The calculation also relies on the assumption that only one type of carrier is injected from one electrode, and none from the other.

The above discussion was also based on the assumption that the only carriers present in the semiconductor are injected carriers. Intrinsic carriers do not contribute to space charge, and thus transport based on intrinsic carriers will follow Ohm's law, which is the case in metals. At very low voltages and current densities this will also be true for real semiconductors, which always have a certain level of intrinsic carriers. We shall thus see a transition from $j \propto V$ to $j \propto V^2$ as the voltage is ramped up.

To discriminate experimentally between barrier type and ohmic injection, it is common to compare $j(V_{\text{bias}})$ characteristics of devices having different thickness $d$. FN tunnelling depends only on the applied field $E = V_{\text{bias}}/d$, thus in a plot of $j$ against $E$ all characteristics will coincide regardless of $d$. In SCLC, $j$ will follow Child's law, $j \propto V_{\text{bias}}^2/d^3$; thus in a plot of $jd$ as a function of $E^2$, all characteristics will coincide. The experimental procedure has to be carried out with symmetric electrodes; e.g., gold/semiconductor/gold for holes and Ca/semiconductor/Ca for electrons. This will ensure single-carrier currents.

SCLC, as described by Equation (6.7c) has been observed for PPV and dialkoxy-substituted PPV. The carrier mobility can be revealed from the slope of the $jd$ versus $E^2$ plot, and in the case of PPV and dialkoxy PPV it was $\sim 10^{-6}\,\text{cm}^2\text{V}^{-1}\text{s}^{-1}$ or less.

#### 6.1.5.4 Charge carrier transport: traps

The most serious deviation from ideal SCLC behaviour is caused by the presence of *traps*, a fact of life in all real semiconductors. A trap is defined as a site with an ionization potential lower than the ionization potential of the bulk material (hole trap), or with electron affinity higher than that of the bulk material (electron trap). The fact that most real organic semiconductors transport only one type of carrier (holes or electrons), with only few *ambipolar* materials known that transport both types, is thought to be the result of carrier-specific deep traps. However, even for the carrier type that is transported, there will be traps.

In a trap, a carrier is immobilized and will therefore contribute to space charge, but not to the current. $j_{\text{SCLC}}$ has to be reduced by a factor $\Theta = n_{\text{trap}}/n_{\text{tot}}$ with trapped and total charge carrier densities $n_{\text{trap}}$, $n_{\text{tot}}$. Alternatively, we may leave Equation (6.7c) unchanged and introduce an effective mobility $\mu_{\text{eff}}$:

$$\mu_{\text{eff}} = \Theta\mu. \tag{6.8}$$

The introduction of $\Theta$, however, is not a simple concept. Firstly, the boundary between trapped and mobile carriers is somewhat blurred for shallow traps, which lie energetically only a few $k_{\text{B}}T$ below the HOMO. Carriers in such traps can be thermally activated back into the conduction band. Secondly, carrier release from deeper trap sites can be field activated, thus making $\Theta$ and $\mu_{\text{eff}}$ complicated functions of the applied voltage. Equation (6.8) also opens the door to some confusion between $\mu$ and $\mu_{\text{eff}}$.

To discuss the effect of traps on current densities, it is instructive to extend the concept of the Fermi level $E_{\text{F}}$ from metals to semiconductors. The Fermi level of a semiconductor (without applied bias) is located halfway between the HOMO and LUMO. This is because the chemical potential for electrons as $T \to 0$ approaches the midgap. In a semiconductor containing mobile and trapped carriers, the Fermi level

(similarly to the HOMO and LUMO) becomes a function of location $x$ and applied bias $V$, rising with higher $V$. Generally, traps will influence the $j/V$ characteristics in a very different manner if the local Fermi level is above or below the trap depth. This may result in a very rapid rise of $j$ with $V$ within a small range of voltages, with power laws $j \propto V^m$ where $m$ is often larger than 10. Nevertheless, in the presence of traps, current density $j$ will always be lower than in the trap-free SCLC case.

## 6.1.6 Polymers versus small molecules

All of our previous discussions on conjugated molecules considered a given, defined molecule. Now we shall discuss aspects that are specific to polymeric organic semiconductors. A polymer is often viewed as infinitely long, but this is often far from true in conjugated polymers. This is due to the, often limited, solubility of conjugated polymers, which results from their stiff backbone. When the polymer reaches its solubility limit during the polymerization reaction, it precipitates and cannot grow any longer. This often happens at relatively low molecular weights. In the organic semiconductor field, there is a tendency to call a material a polymer if it has a distribution of molecular lengths, whereas molecules with a defined number of repeat units (such as 6T) are called oligomers. It does not necessarily mean that the polymer is very long.

### 6.1.6.1 The band gap in a conjugated polymer

One of the most important properties of a semiconductor is its band gap. We therefore need an understanding of what controls the band gap of a conjugated polymer. Let us consider an oligomer series of molecules with a defined length of $n_r$ repeat units, and monitor the band gap as the number of repeat units grows. Obviously, larger $n_r$ means better $\pi$ electron delocalization and smaller band gap. Will the band gap close altogether for a polymer, making the material metallic instead of semiconducting?

Experimentally, this is not observed. Instead, one finds the following scaling of band gap with $n_r$:

$$E_g(n_r) = E_\infty + \frac{E_1 - E_\infty}{n_r} \quad \text{for} \quad n_r < n_{ECS}, \tag{6.9a}$$

and

$$E_g(n_r) = E_\infty + \frac{E_1 - E_\infty}{n_{ECS}} = \text{constant} \quad \text{for} \quad n_r > n_{ECS}. \tag{6.9b}$$

For short oligomers, the band gap reduces proportional to $1/n_r$ but there is a critical $n_r$ ($n_{ECS}$) beyond which $E_g$ remains constant even when $n_r$ continues to grow. In terms of photophysics, $n_{ECS}$ is the boundary between low molecular weight material and polymer. As an example, we look at a fluorene oligomer series. $n$ refers to the number of fluorene units; the absorption maximum (instead of $E_g$) is reported. The $1/n_r$ relationship holds approximately for all data reported; i.e., up to $n_r = 10$ (Figure 6.8). However,

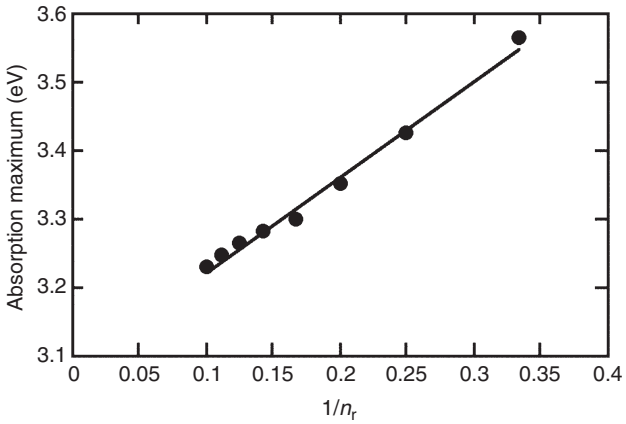


**Figure 6.8** Optical gap plotted as a function of $1/n_r$ for oligofluorenes. The data used in this figure is taken from G. Klaerner and R. D. Miller, *Macromolecules* **31**, 2007 (1998)

extrapolating this relationship, $n_r \rightarrow \infty$ or $1/n_r \rightarrow 0$ leads to an absorption maximum $E_\infty = 3.08\,\text{eV}$. However, a polyfluorene ($n_r \gg 10$) displays a larger absorption maximum of 3.20 eV. This is consistent with $n_{ECS} \approx 12$.

This behaviour can be understood with the concept of the *effectively conjugated segment* (ECS) as initially introduced for PPV.[1] In this picture, a conjugated polymer consists of a string of effectively conjugated segments. At the end of each effectively conjugated segment, one photophysical unit ends and another begins. This is reminiscent of the concept of persistence length $L_p$ in polymer physics, which describes the length over which a polymer chain roughly maintains a given direction; $L_p$ is a measure of chain stiffness. In fact, for polyfluorene, $L_p$ is found to be approximately 11 repeat units, which compares well to $n_{ECS} \approx 12$ repeat units. Hence we see that the presence of conformational degrees of freedom in a polymer chain may limit the coherence of the $\pi$ electron cloud and thus limit effective conjugation length. This enables band gap tuning via chain backbone architecture.

However, conformational disorder is not the only limiting factor of effective conjugation length. The backbone of MeLPPP has no conformational degrees of freedom, and all rings are forced to be coplanar. This provides excellent geometric conditions for $\pi$ overlap. Nevertheless, the MeLPPP effectively conjugated segment length is finite, and is in fact surprisingly short. There is an intrinsic limit to the coherence length of $\pi$-conjugated molecules. As the example of MeLPPP teaches, this limit may be approached sooner for better $\pi$ overlap.

When the ECS is limited by conformational disorder, there will be a certain distribution of ECS lengths within a sample. Consequently, absorption spectra will be the superposition of the spectra of ECSs of slightly different lengths, hence different $E_g$; as a result, the vibronic structure of the absorption spectrum is lost. This is known as *inhomogeneous broadening*. However, in MeLPPP, with its perfectly ordered backbone,

[1] H. H. Hörhold, M. Helbig, D. Raabe, J. Opfermann, U. Scherf, R. Stockmann and D. Weiβ, *Z. Chem.* **27**, 126 (1987).

inhomogeneous broadening is absent; the MeLPPP absorption spectrum displays clearly resolved vibronic structure that mirrors the emission spectrum.

In emission, however, vibronic structure is usually maintained better, even for polymers with a significant degree of conformational disorder. This phenomenon is understood as the result of *exciton diffusion*. An exciton can be transferred from a shorter ECS (larger band gap) to a longer ECS (smaller band gap), but not the other way round. In PPV an exciton can sample a sphere of radius $\sim$5 nm radius before emitting fluorescence. Consequently, for polymers the term 'band gap' becomes even more ambiguous, as the average conjugated segments control absorption, but the lowest band gap conjugated segments control fluorescence.

### 6.1.6.2 Polymer solubility

Much of the appeal of molecular electronics comes from the fact that organic materials can be processed from solution. However, solubility of stiff, elongated molecules rapidly decreases as they get longer, and at the same time, the melting point rises. This is due to the reduced entropy of solution and entropy of melting, a problem that was first encountered probably by Vorländer in the 1920s in his quest to synthesize larger and larger liquid crystalline molecules. Typically, molecules with five or six repeat units such as pentacene or 6T are beyond solubility.

There are two common approaches to this problem. Historically the first, but now not so much in use, is the *precursor approach*. Instead of synthesising a finished, conjugated polymer, one prepares a flexible and soluble precursor polymer, which is processed into a thin film in the envisaged device situation. Then, via a polymer analogous reaction (typically driven by heat), the precursor is converted in situ into a conjugated, and usually insoluble, polymer. A precursor route to PPV based on thermal tetrahydrothiophene elimination is shown in Figure 6.9.

Note that the precursor is a water-soluble polyelectrolyte with a flexible, non-conjugated backbone.

Another approach to soluble, stiff polymers is known from the synthesis of liquid crystalline polymers and can be directly transferred to conjugated polymers. When a stiff backbone is decorated with long, flexible side chains, these side chains gain considerable entropy on dissolution, hence the polymer becomes soluble. This approach has led to the *hairy rod* family of liquid crystalline polymers as well as to a large number of soluble conjugated polymers. Many side chain decorated, soluble conjugated polymers are included in the appendix.

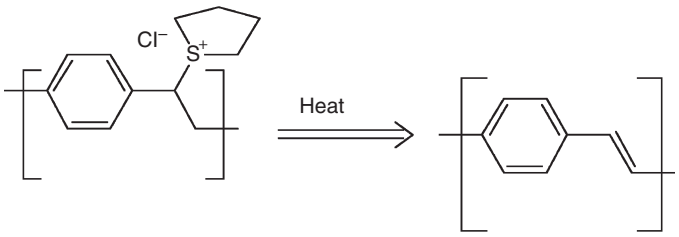


**Figure 6.9** The precursor route to PPV

The resulting soluble conjugated polymers also melt at moderate temperatures, since melting as well as dissolution is entropy-driven. In fact, most conjugated polymers share the basic architecture of stiff backbone with flexible side chains with the hairy rod liquid crystals. It is therefore not surprising that several of them exhibit liquid crystalline phases, most prominently alkyl-substituted PFs and its copolymers such as F8T2 and F8BT.

### 6.1.7 Organic metals?

Considering polyacetylene (PA) in a similar fashion as we did the benzene ring, we find it can have two borderline structures, as shown in Figure 6.10. Again, it is unclear where the double bonds ($\pi$ bonds) should be and, similarly to the benzene ring, they may be completely delocalized along the whole chain. This would lead to metal-like behaviour, as the $\pi$ cloud can move continuously (i.e., in response to moderate fields): inject electrons at one end and they drop out at the other.

However, this does not happen. In the 1950s, Rudolf Peierls proved a general theorem, stating that there can be no one-dimensional metal. Conjugated polymers were not known in Peierls' day, but the correspondence between the then hypothetical 'one-dimensional metal' and materials like PA is obvious.

Peierls showed that a one-dimensional metal would be unstable against a metal–semiconductor transition, the *Peierls transition*. Atoms will move closer to each other pairwise, leaving a wider distance to the next pair, rather than remaining spaced equally (Figure 6.11). Also, the $\pi$ electron density will redistribute to be higher between close

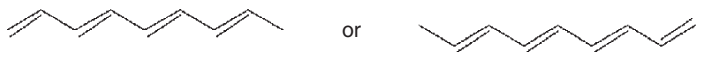


**Figure 6.10** The double bond assignment in PA is ambiguous

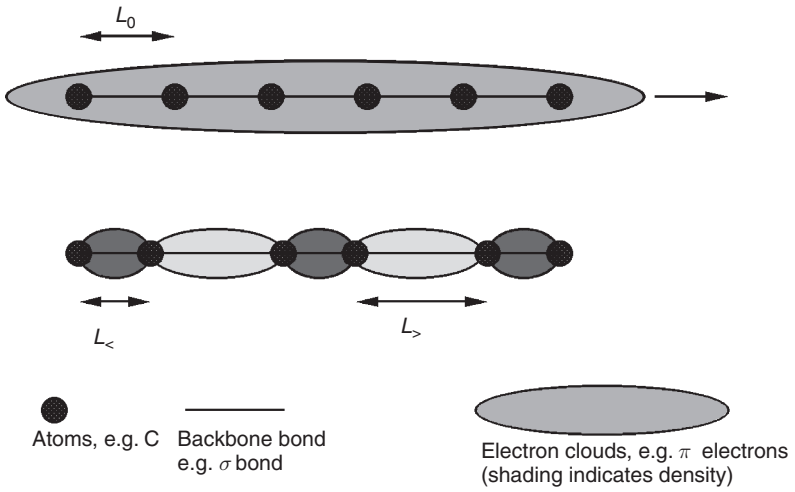


**Figure 6.11** The Peierls transition shown schematically

atoms, and lower between distant atoms. There will be a limit to the pairing due to the elastic distortion of the one-dimensional chain. This 'elastic force' results from the $\sigma$ bonds. The balance between these forces is given by a bond alternation parameter $\delta$:

$$\delta = \frac{L_> - L_<}{L_> + L_<} \tag{6.10}$$

The description with alternating single/double bonds having different bond lengths is therefore adequate. Note that the size of the unit cell has doubled due to the Peierls transition. The number of valence electrons in the double unit cell is now even, hence the material can be a semiconductor. In fact, the doubling of the unit cell opens up a band gap between the HOMO and the LUMO, which refers to an antibonding state, where the $\pi$ electron density is high between the long bonds and low between the short bonds.

It should be noted that a Peierls transition would only lead to band gaps of order 0.2 eV in a conjugated polymer, whereas gaps of order 3 eV are often found. The Peierls transition is an oversimplification. The true band gap is due to the simultaneous presence of a *Mott–Hubbard* transition. Nevertheless, McDiarmid, Sarikawa and Heeger were awarded the 2000 Nobel prize in chemistry for the discovery of synthetic metals. As so often in the applied sciences, a theoretical limit can be sidestepped rather then overcome. Their discovery will be discussed in Section 6.2.1.

## 6.2 APPLICATIONS AND DEVICES

The expected massive added value of organic semiconductor products once they are manufactured in bulk quantities and sold competitively on the markets has fuelled the recent rapid development in organic semiconductor materials. It is therefore impossible to sensibly discuss materials without devices and applications. We will see how the demands on new or improved materials originate in the attributes and requirements that the respective application demands. Therefore we will here introduce the key applications and devices that are being addressed currently. This discussion excludes the one application that is already dominated by organic semiconductors, namely, photoconductors for xerography and laser printers.[2]

### 6.2.1 Synthetic metals

Typical examples of so-called synthetic metals are polyacetylene (PA), polydiacetylene (PDA), polyaniline (PANi), and poly(3,4-ethylene dioxythiophene) (PEDOT). In their pristine state, these materials are organic semiconductors and the term 'synthetic metal' is not entirely appropriate. Synthetic metals become quasi-metallic only as a result of *doping*. Doping with heteroatoms (electron acceptors near the VB, or electron donors

[2] This topic is covered in much detail in, for example, P. M. Borsenberger and D. S. Weiss, *Organic Photoreceptors for Imaging Systems*, Marcel Dekker, New York, 1993.

near the CB) is a well-known concept in inorganic semiconductors, and can make a semiconductor quasi-metallic at room temperature, although strictly, the defining characteristics of a metal are not met.

Doping of organic semiconductors is somewhat different as it involves a chemical reaction between semiconducting polymer and dopant, wherein the dopant changes the number of $\pi$ electrons in the backbone. Both redox and acid/base reactions between semiconductor and dopant have been used successfully; dopant concentrations of between 1% and 50% are typically used. When referring to a synthetic metal, it is not sufficient just to quote the (intrinsically semiconducting) polymer used, but also the type and concentration of dopant, together with the relevant processing conditions. Room temperature conductivities in the range $10^{-3}$ to $10^{7}\,\mathrm{S\,m^{-1}}$ have been reported; the highest of these conductivities are comparable to those of metals: For example, gold has a conductivity of approximately $5 \times 10^{7}\,\mathrm{S\,m^{-1}}$ at room temperature.

Historically, the first discovery of metallic conductivity in doped PA was an accident. An iodine-containing catalyst was used for PA synthesis. By accident, 1000 times the intended catalyst concentration was added. It turns out that iodine is a useful (redox) dopant for PA, and it was this fact which led to the award of the 2000 Nobel prize in chemistry.

#### 6.2.1.1 Solution-based synthetic metals

The first synthetic metals existed in the form of intractable films only. The breakthrough from laboratory curiosity towards industrial application for synthetic metals came with the advent of modern, aqueous solution based preparations that can be applied to most surfaces, or can be processed by an inkjet printer. Doped PANi and PEDOT are now commercially available in that form. The fact that synthetic metal preparations are water based, but do not dissolve in common organic solvents, makes them very attractive for use as metallic electrodes or interconnects in conjunction with organic semiconductors, which are typically processed from organic solvents but do not dissolve in water.

As the outstanding example, we here discuss the manufacture and applications of PEDOT preparations. For high conductivity, PEDOT is acid doped (rather than redox doped) with poly(styrene sulfonic acid) (PSS) to form the highly conductive PEDOT/PSS complex. The key idea to arrive at a water-based preparation is to synthesize PEDOT from EDOT monomer in an aqueous medium that already contains the PSS. The reaction is shown schematically in Figure 6.12.

Note how the chemical bonding pattern of EDOT/PEDOT changes under acid doping: A C=C $\pi$ bond opens up and the C bonds to a proton donated by the acid. As a result, there is a net positive charge on the PEDOT chain that will strongly attract the negative charge left on the acid. Since this happens at many points along the chain, PEDOT and PSS become closely intertwined and float as a fine dispersion or colloid in water, rather than precipitate. Also, an unpaired $\pi$ electron remains on the main chain that is highly mobile along the chain. The removal of one $\pi$ electron from the HOMO is akin to the removal of one electron from an inorganic semiconductor VB by an electron acceptor just above the VB level, but results from a chemical reaction, not the presence of a heteroatom.

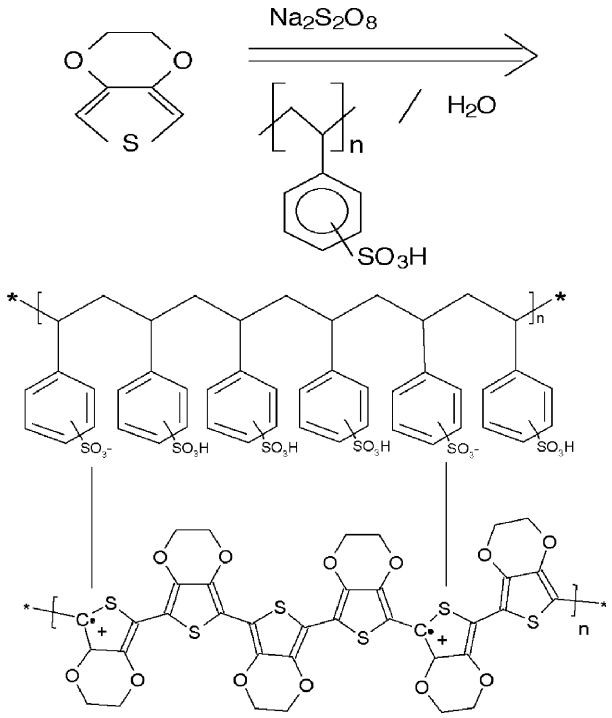


**Figure 6.12** The synthesis of PEDOT from EDOT in aqueous medium in the presence of poly(styrene sulfonic acid). $Na_2S_2O_8$ acts as oxidizing agent for EDOT polymerization

Films cast from commercial PEDOT/PSS solution (Bayer trade name Baytron P) display resistivities typically between $10^{-2}$ to $10^{-3}\,\Omega\,m$; i.e., conductivities of between 100 and 1000 S $m^{-1}$. For surface coating applications, it is common to quote the *sheet resistance*, expressed in $\Omega/\square$ (ohms per square). Sheet resistance is defined as resistance between two electrodes of length $L$ separated by distance $L$; this is independent of $L$. A typical sheet resistance for cast PEDOT/PSS is 1 $M\Omega/\square$ when 20 $g/m^2$ material is used. Recently, PEDOT/PSS coated polyester sheets have become available with much lower sheet resistance of order 1 $k\Omega/\square$ (Agfa Orgacon).

### 6.2.1.2 Applications of synthetic metals

PEDOT/PSS was originally developed as an antistatic coating for photographic films. Large-scale film processing, or 'development', leads to static charging, with potentials up to several thousand volts. Discharge sparks can expose the film. Similarly, static charges have to be avoided in the packaging of electronic components. A PEDOT/PSS coating with surface resistance of $\sim$1 $M\Omega/\square$ is sufficient to disperse charges before high voltages build up. Today more than $10^8$ $m^2$ per year of photographic film is coated with PEDOT/PSS. Another interesting application of PEDOT/PSS is as counterelectrode in anodically prepared electrolytic capacitors.

In the context of organic semiconductor devices, the most interesting applications of PEDOT/PSS are as coatings for the commonly used ITO anodes, and as printable electrodes and connectors in organic transistor circuits. PEDOT/PSS has a very high work function ($\Phi \approx 5.2$ eV), considerably higher than that of ITO ($\Phi \approx 4.7$ eV). Thus, ohmic hole injection can be achieved for many common organic semiconductors from a PEDOT/PSS coated anode, when it would be non-ohmic from uncoated ITO. It is tempting to replace ITO on glass anodes altogether by flexible, transparent Agfa Orgacon sheets. These can be patterned by a photolithographic etching procedure, and are expected to have a great impact in the development of novel small-scale organic electroluminescent (EL) devices. However, the sheet resistance is still too large for large-scale displays.

In the field of organic transistors, the impact of PEDOT/PSS results from the option to process from solution, in particular via inkjet printing. PEDOT/PSS can serve as gate metal, as inkjet printed PEDOT/PSS source and drain electrodes, and as printed vias (interconnects).

## 6.2.2 Organic field effect transistors

The aim of organic FET (OFET) research is not to outperform current inorganic semiconductor processors in terms of integration density or processing speed. Instead, the idea is to make low-performance integrated circuits based on organics at extremely low cost, cheap enough to be discarded after single use (disposable electronics). One target application is an electronic RF price tag on a food wrapper that a supermarket checkout can read remotely. The target of extremely low cost imposes strict limits on the processing technologies that can be used practically. For example, any vapour deposition step in the device manufacture has to be avoided; vacuum is too expensive.

### 6.2.2.1 The principle of FET operation

Figure 6.13 is a sketch of a thin film FET with electric connections. A voltage between source (S) and drain (D), called the *drain* or *source–drain voltage* $V_D$, attempts to drive a current through the semiconducting transistor channel. However, a *drain current* $I_D$ will only flow if there are mobile charge carriers in the channel.

A *gate voltage* $V_G$ will extract carriers from the source into the semiconducting channel. However, since the *gate dielectric* is an insulator, these carriers cannot reach the gate metal. Instead, they will form an *accumulation layer* at the channel–insulator interface. The channel semiconductor thus gets doped by applying $V_G$. Unlike chemical doping, this is quickly reversible, simply by switching off $V_G$. $V_G$ switches channel conductivity, in some (desirable) cases by several orders of magnitude. Accordingly, $I_D$ at a given $V_D$ will change with $V_G$; the FET is an *electronic switch*. Note that an OFET is switched on by applying $V_D$ and $V_G$ of equal polarity *opposite* to the sign of the mobile carriers. Thus, OFETs can easily be used to determine the type of carriers a particular material sustains. If positive $V_G$, $V_D$ switch the transistor on, then the carriers are negative (electrons); if negative $V_G$, $V_D$ are required, then the carriers are holes. To minimize injection barriers from source to the semiconductor, high work function

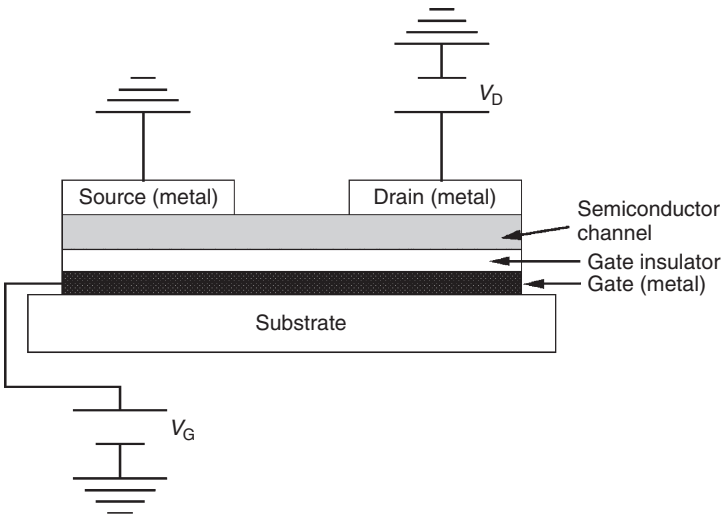


**Figure 6.13** A FET with bottom-gate architecture. Transistors may also be built the other way round, with top-gate architecture

metals such as gold or PEDOT/PSS are used for hole channel semiconductors, and low work function metals such as Ca for electron channel semiconductors.

#### 6.2.2.2 Quantitative description of FET operation

To characterize the gate and source – drain voltage-dependent drain current in a FET beyond the qualitative on/off description, usually two types of measurements are carried out: the *output* and *transfer* characteristics. The output characteristic of a FET is the family of curves $I_D$ against $V_D$ at different $V_G$, but $V_G$ fixed during every single $V_D$ scan. The transfer characteristic is the family of $I_D$ against $V_G$ curves at different $V_D$, but $V_D$ fixed during every single $V_G$ scan.

The following formulae apply (the derivation is rather technical):

$$I_D = \frac{Z}{L} C_i \mu (V_G - V_T) V_D \text{ for small } V_D \ (|V_T| < |V_D| \ll V_G) \tag{6.11a}$$

$$I_D = I_{sat} = \frac{Z}{2L} C_i \mu (V_G - V_T)^2 \text{ for large } V_D \ (V_D \geq V_G). \tag{6.11b}$$

where $Z/L$ is the channel width/length, $C_i$ is the capacitance per unit area of the insulator, $V_T$ is a threshold voltage, and $\mu$ is the charge carrier mobility. For a dielectric, $C_i = \varepsilon_r \varepsilon_0 / d$, where $\varepsilon_r$ is the dielectric constant and $d$ is the film thickness. $\varepsilon_r$ describes how much a dielectric shields the applied field. The large $V_D$ regime is known as the *saturation regime*, $I_D$ does not rise with higher $V_D$ any more but levels off at a ($V_G$-dependent) saturation current $I_{sat}$. Saturation will be reached at $V_D \approx V_G$, because at $V_D = V_G$ the field between gate and drain is zero, and the accumulation layer pinches

off. The theory of the threshold voltage $V_T$ is rather intricate, and has specific differences between organic and inorganic FETs.

From experimental transistor characteristics, the charge carrier mobility can be determined with the help of Equation (6.11). A robust method is to plot $\sqrt{I_{sat}}$ against $V_G$ (for $|V_D| > |V_G|$), which should produce a straight line with a slope directly related to $\mu$.

For a low-noise measurement, we wish to have a relatively high drain current, which at given mobility, dielectric and operating voltages is determined by the geometry factor, written as $Z/L$. The maximum geometry factor leads to higher currents that can be measured more comfortably. Often, source and drain are therefore evaporated through an interdigitating comb shadow mask, with many channels in parallel. Practical transistors, however, have to be small and should work with only one channel. Also, $L$ controls the time $\tau$ that a carrier requires to cross the channel:

$$\frac{1}{\tau} = f \approx \frac{\mu V_D}{L^2}. \tag{6.12}$$

$L$ enters the equation as $L^2$; one factor of $L$ comes from the linear dependence of the transit time of carriers through the channel on $L$, the other factor of $L$ arises from the dependence of the electric field on $1/L$. $\tau$ is one of the limiting factors of switching speed. A genuine engineering challenge is therefore to achieve, at low cost, the smallest possible $L$ without inadvertently creating electrical short circuits.

#### 6.2.2.3 Requirements on OFET materials

Good OFETs should display high drain current at low drain and gate voltages, without relying on the optimized geometry factor; they should also have high on/off ratios, which means drain current at $V_G = 0$ should be extremely low. We will discuss the materials requirements for the different components of an OFET to achieve these goals.

*Requirements on OFET semiconductors*

Equations (6.11) and (6.12) underscore the importance of high carrier mobilities for good drain current at moderate gate and drain voltages. Hence much effort in synthetic chemistry and physical chemistry is geared towards high-mobility materials. In this section we shall discuss several aspects of charge carrier mobility in organic semiconductors. We assume throughout that we are in the incoherent (hopping) transport regime.

In an OFET, carriers are confined to a very thin interface layer between gate insulator and semiconductor, typically only ~5 nm thick. The resulting interface mobility may differ from the bulk mobility as measured, for example, by the time-of-flight (ToF) method. The approach closest to practical application is thus to build an OFET, measure saturated transfer characteristics, and determine $\mu$ from the $\sqrt{I_{sat}}$ versus $V_G$ plot.

In a given material, carrier mobility can depend very strongly on the material morphology, which in turn may change as a result of different preparation conditions. Besides the synthesis of suitable materials, the control of morphology is the key to high mobility. Hence there is no such thing as *the* mobility of a material with a given chemical formula. In fact, there are charts for a few materials showing the evolution of carrier mobility over the years as a result of improved preparation technique.[3] Therefore a wide range of data may be quoted for the same material. This is meant as a caution before considering a few examples in Table 6.2.

Different applications require minimum mobilities of 0.01 to 0.1 $cm^2V^{-1}s^{-1}$. The high mobilities found for some single crystals (e.g., single-crystal pentacene in the coherent transport regime), or for certain thin films carefully deposited onto specific substrates under carefully controlled conditions, are often not useful for practical devices. The challenge is to develop materials that display reasonably high mobilities after a realistic deposition method, such as inkjet printing. As a rule of thumb, thiophene or thiophene-containing materials are the most promising, both for low molecular weight materials (6T and soluble derivatives thereof) or polymers (polyalkylthiophenes

**Table 6.2** Mobilities for various molecules at room temperature. The molecules are either hole transporters (h) or electron transporters (e)

| Material | Morphology | $\mu$ ($cm^2V^{-1}s^{-1}$) | h/e |
|---|---|---|---|
| Pentacene | Large single crystal, vapour deposited, no grain boundaries, along *c* axis (crystallographic axis perpendicular to the molecular plane) | 100 | h |
| Pentacene | Spin coated | 0.001 | h |
| Pentacene | Evaporated onto substrate, substrate at room temperature | 0.002 to 0.03 (different studies) | h |
| Pentacene | Evaporated onto substrate, substrate at 120 °C | 0.62 | h |
| F8T2 | Aligned liquid crystal, parallel to alignment | 0.01 to 0.02 | h |
| F8T2 | Aligned liquid crystal, orthogonal to alignment | 0.001 to 0.002 | h |
| PPV | Several morphologies and methods | $10^{-7}$ to $10^{-4}$ | h |
| PAT | Regioregular, edge-on substrate | 0.1 | h |
| PAT | Regioregular, face-on substrate | 0.001 | h |
| 6T | Single crystal | 0.1 | h |
| 6T | Polycrystalline | 0.02 | h |
| DH6T | 6T with ($\alpha, \omega$)-dihexyl endchains | 0.05 | h |
| $C_{60}$ | In ultrahigh vacuum | 0.08 | e |
| $C_{60}$ | Under air | $<10^{-5}$ | e |

[3] See, for example, Figure 14.13 in G Hadziioannou and P F van Hutten (eds.), *Semiconducting Polymers*, Wiley-VCH, Weinheim, 2000.

or F8T2). Generally, a high degree of molecular order such as regioregularity in polyalkylthiophenes, or liquid crystalline alignment in F8T2, does result in enhanced mobilities. However, crystallization is usually undesirable. Organic single crystals may display very high mobility coherent transport but, for realistic preparation techniques, materials end up in a polycrystalline morphology, or for polymers, partially crystalline morphology. A crystalline grain boundary, or the interface between a crystalline and an amorphous region, typically represents a deep trap that must be avoided, as it reduces effective mobility $\mu_{\text{eff}}$ (6.8). Since the channel current is localized in a very thin interface layer close to the gate insulator, trap states at the gate insulator surface may be just as bad as in the semiconductor. The preparation (i.e., synthesis and processing) of materials with high degrees of intra- and inter-molecular order, but without crystallinity, is one of the major challenges in the design of OFET materials.

Another requirement is a certain degree of environmental stability. As an example from Table 6.2, $C_{60}$ may display very high electron mobilities when oxygen is strictly excluded, but electron mobility is poor in the presence of oxygen. Low-cost devices cannot be encapsulated in a way that excludes oxygen completely, thus $C_{60}$ plays no role in current OFET technology.

Generally, it is fair to say that p-type (hole-transporting) OFET materials are now developed to a much higher state of the art than n-type (electron-transporting) materials. $C_{60}$ will not plug that gap, owing to its oxygen sensitivity. A single OFET can operate with a p-type channel, and it would thus be tempting to abandon research into n-type materials altogether. However, the popular CMOS (complementary metal oxide semiconductor) architectures of inorganic semiconductor circuits require n-type and p-type transistors on the same chip. The desire to mimic them with OFETs means that the quest continues for a high-quality n-type OFET material.

High carrier mobility ensures that, for the operation of an OFET as a switch, relatively moderate values of $V_G/V_D$ lead to a decent $I_D$, and the switch can be switched on easily. However, this is not the only requirement on an OFET. A switch is useless if it cannot be switched off as well as on. An off-current may result if the OFET semiconductor is permanently (chemically) doped, thus giving channel conductivity even at $V_G = 0$. Practically, the on/off ratio can be read directly from the transfer characteristic with $V_D$ applied at the level at which the respective device is meant to operate, and $V_G$ applied or switched off again at whatever level is available. The required on/off ratios depend on the application; e.g., an on/off ratio of $10^6$ is required for active matrix addressed liquid crystal displays. For high on/off ratios, OFET semiconductors have to show high mobility $\mu$ at very low (intrinsic) conductivity $\sigma$. However, since $\sigma = nq\mu$, where $n$ is the (intrinsic) charge carrier density, a high mobility (desirable) implies a high conductivity (undesirable) unless we keep $n$ extremely low, emphasizing the need for ultrapure materials to avoid accidental doping. Here vapour-deposited films have the edge over solution processing, because vapour deposition is a purification step (an evaporation–condensation cycle is similar to recrystallization). Ultrapure preparation is a great challenge to synthetic chemistry. As an example, the conventional preparation of 6T couples two 3T by oxidative dimerization with ferric chloride ($Fe(III)Cl_3$). However, traces of ferric chloride make it into the final product, and chloride is known to be an oxidative dopant; for example, $Cl^-$ can turn PA into a synthetic metal. This intrinsic doping leads to unwanted conductivity, and OFET grade 6T is now made by coupling lithiated 3T

with ferric acetylacetonate instead. Thiophenes also suffer from oxygen exposure, but in a different way from $C_{60}$; thiophenes form a weakly bound charge transfer complex with molecular oxygen that acts as dopant, leading to unwanted conductivity. This limits the practical usefulness of the otherwise very promising thiophenes. A certain level of protection is afforded in the top-gate architecture.

*Requirements on the other OFET materials*

The source metal should show good carrier injection into the semiconductor. This favours high work function metals such as gold (Au), or indeed PEDOT/PSS, which is a boon for all-plastic electronics. Usually it is convenient to use the same material for the drain metal as well. Then the source and drain become interchangeable and are defined by the wiring. The electrical requirements for the gate metal are not very strict. The sheet resistivity need not be extremely low, because ideally no current flows to the gate. This again favours a synthetic metal.

The gate insulator is critical and may be the least well developed aspect of OFET technology. We desire transistors that can operate with rather low gate voltages: in a simple application, no high-voltage source will be available. To achieve low gate voltage switching, we require high capacitance per unit area, $C_i$, for the gate insulator. Since $C_i \propto \varepsilon_r/d$, a good gate insulator should provide pinhole-free insulation at very low thickness, have a high dielectric constant $\varepsilon_r$, have high electric breakdown strength, and be insoluble in the solvent of the channel material, because channel and insulator have to be prepared on top of each other. The solubility requirements are usually fulfilled by insulating polymers such as poly(vinyl phenol) (PVP) or poly(methyl methacrylate) (PMMA) that dissolve in alcohols, but not in less polar organic solvents. Unfortunately, the dielectric constant of organic materials is usually rather low ($\varepsilon_r \leq 4$), and relatively thick layers are required ($d \geq 300\,\text{nm}$) to obtain pinhole-free films. The inorganic gate insulator $SiO_2$ that is conventionally used for inorganic chips also has a rather poor dielectric constant ($\varepsilon_r = 3.9$) but provides insulation in much thinner films. Other inorganic insulators have a much higher $\varepsilon_r$ ($\varepsilon_r = 9$ for $Al_2O_3$, $\varepsilon_r = 22$ for $ZrO_2$, $\varepsilon_r = 23$ for $Ta_2O_5$).

Of course, OFETs can be (and have been) built with $SiO_2$ and other inorganic gate insulators (e.g., $Ta_2O_5$), and these devices display lower gate voltage switching than comparable devices with organic insulators. However, these gate insulators are more expensive, so they are not an option for disposable electronics. Hence, there is room for improvement.

### 6.2.2.4 Integrated circuits based on OFETs

The discussion so far has focused on the properties of single OFETs, however, logic circuits always require a large number of transistors wired up to each other. The desire for high packing density is one driving force to achieve OFET architectures as small as possible. The other is a direct consequence of Equations (6.11) and (6.12), which show that a short channel length $L$ is required for fast OFETs with high drain current at moderate $V_G$ and $V_D$.

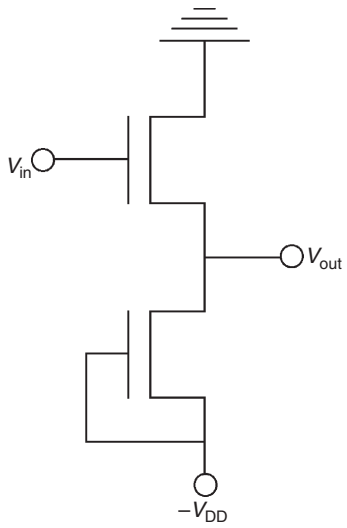


**Figure 6.14** The principle of an inverter

The basic building block of a logic circuit based on FETs is the *inverter*. It can be built from two FETs, as shown in Figure 6.14. $-V_{DD}$ is a supply voltage. When $V_{in}$ is high, $V_{out}$ will be low, and vice versa; the inverter performs the logical operation NOT. Note that the drain of the second FET is connected to its gate. This introduces a key feature of circuits as compared to individual transistors, which poses a considerable challenge to device engineering: to make useful circuits, there needs to be interconnects from the source/drain level to the gate level, going through the semiconducting channel/ and through the gate insulator. These interconnects are called *vias*. The preparation of via interconnects represents another great engineering challenge for the manufacture of practical organic circuits. Patterning on the source/drain and the gate level are also necessary. Currently, two approaches to plastic circuit engineering are competing: photolithography and inkjet printing techniques.

The group at Philips Research Laboratories in Eindhoven have used camphor sulphonic acid doped PANi as the source/drain and gate metal. To pattern the source/drain level, a photoinitiator molecule was added; on exposure to UV light, it cross-linked the PANi and led to an increase in PANi resistivity of 10 orders of magnitude – practically turning PANi into an insulator. Hence the negative of a mask could be patterned into the PANi. The insolubility of PANi in organic solvents was crucial for deposition of the semiconductor poly(thienylene vinylene) (PTV) and the gate insulator PVP. Vias were punched mechanically with pins, providing sufficient mixing between the gate and source/drain PANi to give electrical contact. A 15-bit all-plastic programmable code generator was demonstrated that still worked when the device was sharply bent.

The photolithography approach to organic electronics has its limitations. Apart from probably being too costly, when plastic substrates are used, dimensional stability is not given over large areas; there may be some warp between the gate and source/drain level, which leads to a loss of registration. An alternative approach that does not suffer from this problem uses inkjet printing to put an inverter in the top-gate architecture. The source/ drain and gate were made from PEDOT/PSS, with F8T2 as channel semiconductor and

PVP as gate insulator. Since the inkjet printer can be mounted with an optical system, local registration between source/drain and gate is possible and, in principle, circuits of unlimited size can be manufactured. Importantly, an effective method for making via holes was also devised. When a droplet of plain solvent is printed onto an existing semiconductor, it will dissolve the semiconductor. When the solvent then evaporates, semiconductor is deposited mainly at the edges of the droplet. This phenomenon is known as the 'coffee stain effect'. Effectively, the solvent droplet has etched a hole into the semiconducting film which can then be filled with a synthetic metal droplet to make a via interconnect.

## 6.2.3 Organic light-emitting devices

The huge optical display market is currently dominated by cathode ray tubes (CRTs) and liquid crystal displays (LCDs). Both technologies are rather dated and have severe drawbacks; for example, CRTs are bulky and consume large amounts of energy, and LCDs are passive devices that require backlighting and often suffer from poor viewing angles. Replacing them with organic light-emitting devices (OLEDs) is tempting commercially as well as technologically, and the desire to do so has provided much of the momentum for organic semiconductor research throughout the 1990s.

### 6.2.3.1 Overview of basic processes

As discussed in Section 6.1.4, during fluorescence excitons are created by the absorption of light before fluorescing, whereas during EL excitons are created by electron and hole polaron capture. Polarons first have to be injected from the electrodes, and migrate towards each other. They then form an exciton that can sometimes decay under the emission of light. Figure 6.15 shows the basic architecture of an organic light-emitting device (OLED). The variety of electrical and photophysical processes involved are summarized in Figure 6.16.

Assuming that carrier traps can be avoided, charge carrier mobility is considerably more important for OFETs than it is for OLEDs. This is simply because of the much shorter distances carriers need to travel across a device to the other electrode. In the planar OFET geometry, typical channel lengths are several micrometres, while in the vertical OLED architecture, layer thickness is of order $\sim$100 nm. Apart from special devices, such as organic lasers or OLEDs that emit short pulses, we can therefore use conjugated materials with much lower carrier mobilities in OLEDs than in OFETs. The PPV family of OLED materials is a case in point. However, to operate OLEDs as efficiently as possible, all processes shown in Figure 6.16 need to be optimized as discussed below.

### 6.2.3.2 Bipolar carrier injection

The basic physics of carrier injection from electrodes into organic semiconductors were discussed in Section 6.1.5.1. The key feature that sets apart an OLED from an OFET is that an OFET can operate with one type of carrier, whereas an OLED always requires

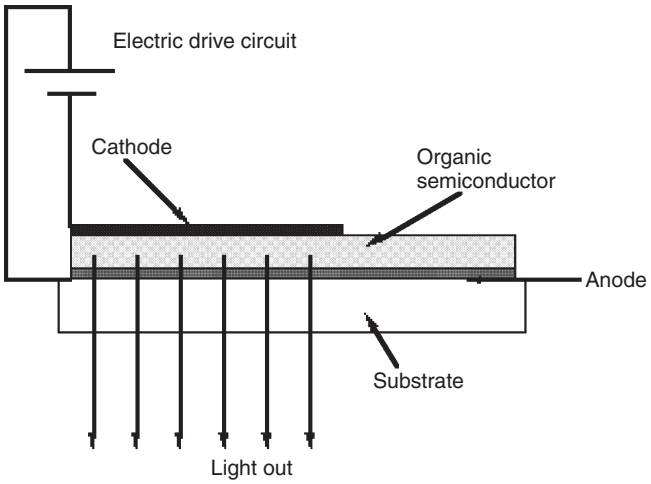


**Figure 6.15** OLED architecture

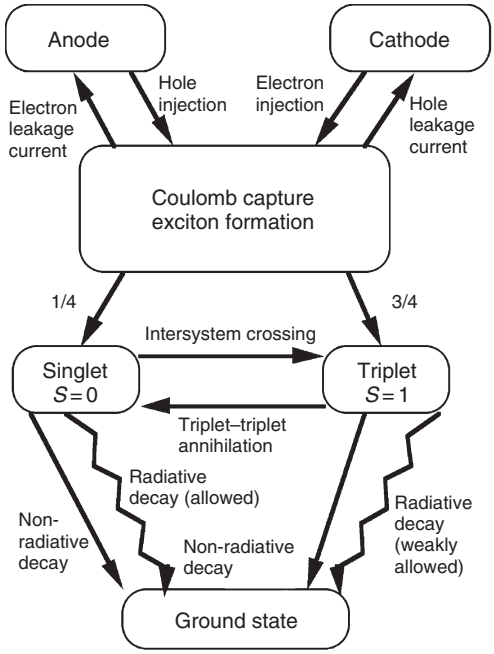


**Figure 6.16** A chart describing the formation and decay of excitons in organic electroluminescent devices. Adapted from D. D. C. Bradley, *Current Opinion in Solid State & Materials Science* **1**, 789 (1996)

both electrons and holes to be injected, otherwise no excitons can form. Ideally, we wish to have ohmic injection of holes at the anode, and electrons at the cathode, simultaneously. As a consequence, OLEDs will use unlike metals for the anode and cathode, namely a high work function anode and a low work function cathode, whereas OFETs

normally use the same metal for source and drain electrodes. This defines a *forward bias* and a *reverse bias* for OLED operation. However, it is still difficult to achieve ohmic (i.e., barrier-free) injection at both electrodes for a given organic semiconductor.

The breakthrough towards efficient organic EL devices came from a device engineering approach at the Eastman Kodak Research Laboratories, rather than from materials development. Here a bilayer device was manufactured that consisted of a low ionisation potential, hole-transporting diamine layer and a high electron affinity, electron-transporting $Alq_3$ layer (see the Appendix), which is also an efficient green emitter. This idea has since been widely adapted and modified. Figure 6.17 shows the level diagram for a (fictitious) double-layer device consisting of a hole-transporting layer (HTL) and an electron-transporting layer (ETL). Both layers are assumed to have a band gap $(I_p - E_a) = 2.5\,\text{eV}$, however the HTL has lower $I_p$ than the ETL, and the ETL has higher $E_a$ than the HTL. It is immediately obvious that a single-layer device using either HTL or ETL alone would necessarily have one large (1 eV) injection barrier. In the double-layer architecture both barriers are moderate (0.5 eV).

In addition to the injection barrier, both holes and electrons will encounter an internal barrier at the HTL–ETL interface, but this barrier is not detrimental to device performance. Instead, it can help to improve the balance between the electron and hole currents. Assuming a slightly smaller injection barrier for holes than for electrons, or a higher hole mobility than electron mobility, a carrier imbalance with a larger hole current than electron current would be expected even in a bilayer device. However, since holes will encounter an internal barrier, they will not simply cross the device and leave at the cathode as a 'blind' leakage current. Instead, they will accumulate at the interface, where they represent a positive space charge. The effect of the field resulting from that space charge is to improve charge carrier balance. Firstly, it will impede the further injection of majority carriers (holes) from the anode, and secondly, it will enhance the injection of minority carriers (electrons) from the cathode. Also, excitons

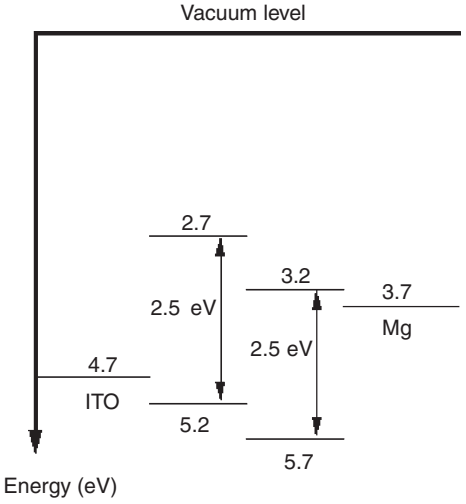


**Figure 6.17** Energy level diagram of a fictitious double-layer device, using an ITO anode and a magnesium cathode

will form at the internal interface, far away from the electrodes. Cathodes in particular have been associated with exciton quenching (i.e., radiationless exciton decay); this is avoided by placing exciton formation in the centre of the device rather than close to the cathode.

As the Kodak Group used small molecules, bilayers could readily be manufactured by subsequent evaporation. This approach has been extended to sophisticated multilayer architectures, yielding brightnesses of over $10^5 \mathrm{cdm}^{-2}$ and external quantum efficiencies of over 7% to date.

With polymeric organic semiconductors, vapour deposition is not an option, devices have to be prepared by spin-casting instead. Multilayer architectures are harder to realize with spin-casting than with vapour deposition, because of the need for orthogonal solubilities (i.e., the solvent used for a particular polymer layer must not cause the dissolution of the preceding layer). To sidestep solubility problems, in principle a precursor route may be employed, where the first layer is prepared from a soluble precursor polymer that then is converted in situ into a conjugated and completely insoluble polymer. This has been successfully employed for hole-transporting PPV and electron-transporting CN-PPV double-layer polymer OLEDs. However, lengthy in situ thermal conversion under high vacuum is awkward, and the use of precursor polymers has generally fallen out of favour following the advent of soluble conjugated polymers.

A very favourable approach has recently emerged that combines the ease of injection into a double-layer device with the simplicity of solution processing. In that approach, a single layer of a blend of a hole-transporting and an electron-transporting conjugated polymer, namely poly(dioctyl fluorene) (PFO) and F8BT, is spin-cast in one single preparation step. As spin-casting implies the very rapid formation of a solid film from solution, the two polymers have little time to phase separate and a solid film may result where both polymers remain intimately mixed. Such a mixture has been termed a bulk heterojunction, and the preparation and morphology control of hole/electron transporting blends is the focus of much current research, mainly with a view to photovoltaic applications of organic semiconductors. Holes are injected and transported into the (majority component) PFO, but can be transferred easily to F8BT, as it has similar ionization potential. However, F8BT has poor hole mobility due to hole-specific traps. Instead, it has rather high electron affinity and displays comparatively good (albeit dispersive) electron transport. Thus electrons are mobile on the F8BT chain until they encounter a trapped hole. With some further device improvements, highly efficient ($>4\,\mathrm{cd\ A}^{-1}$) and low onset voltage ($\sim 3\,\mathrm{V}$) OLEDs have been prepared from such blends.

#### 6.2.3.3 Exciton formation

When both hole and electron polarons have been injected into a device, and they drift towards each other under the applied voltage, they will combine into excitons that may emit light. The physics of this process is discussed in Section 6.1.4.2.

At first sight, it appears that exciton formation in multilayer architectures is hindered by the internal barrier encountered by carriers of either type at the HTL–ETL interface. However, this is generally not the case. Excitons in organic semiconductors generally display exciton binding energies $E_b$ of 0.1–0.3eV. When a carrier has to overcome an internal barrier to form an exciton, this may require a certain amount of energy. However, on exciton formation, $E_b$ is instantly refunded. Effectively, the internal

barrier is reduced by $E_b$. Thus, majority carriers remain stuck at an internal barrier and redistribute the internal field in the favourable way discussed above, until a minority carrier arrives at the interface. As soon as a minority carrier is available, exciton formation is then helped by the effective barrier reduction $E_b$. High $E_b$ also stabilizes excitons against dissociation and non-radiative decay.

In bulk heterojunction blends, one carrier has to transfer from one chain to another to form an exciton. This will be the type of carrier for which the energy level offset of the ionization potentials ($|\Delta I_p|$) or the electron affinities ($|\Delta E_a|$) is smaller. Let us call the smaller of these energies the transfer energy, $E_t$. Two very different scenarios emerge for the case $E_t < E_b$ as opposed to $E_t > E_b$. In the former case, formation of excitons from polarons will be favoured, while in the latter case, the dissociation of existing excitons into polarons will be preferred. In the case of F8/F8BT blends introduced previously, exciton formation is clearly favoured, and such blends are useful for OLED applications. In other hole/electron transport material blends, such as poly(alkyl thiophene)/perylene tetracarboxyl diimide blends, exciton dissociation is favoured, which makes such blends attractive for use in photovoltaic devices. While measurements of $|\Delta I_p|$, $|\Delta E_a|$ and $E_b$ with sufficient precision to predict exciton formation or dissociation are usually not available, there is a simple experimental approach to decide which is the case. If in a blend the fluorescence intensity is much reduced compared to the pure components, then excitons are separated efficiently due to the presence of the blend partner.

#### 6.2.3.4 Optimizing OLED efficiency

The discussion so far outlines the strategy towards OLED devices with balanced carrier injection and quantitative exciton formation that can be driven at low voltage. The formidable challenge that remains is to maximize the amount of light generated from the excitons. It is obvious that we require a material with a high luminescence quantum yield. However, the formation of normally non-emissive triplet excitons presents an unwanted limit on OLED efficiency, and several approaches to overcome this have been explored.

Generally, $\eta_{EL}$ and $\eta_{PL}$ are related via:

$$\eta_{EL} = \frac{\sigma_S/\sigma_T}{\sigma_S/\sigma_T + 3}\eta_{PL}, \tag{6.13}$$

where $\sigma_S$ and $\sigma_T$ are the polaron capture cross sections for singlet and triplet exciton formation, respectively. The naive assumption $\sigma_S = \sigma_T$ leads to $\eta_{EL} = \eta_{PL}/4$.

*Enhanced singlet exciton formation*

Comparisons of EL and PL quantum efficiencies have yielded contradictory results. Some experiments confirm that $\eta_{EL} = \eta_{PL}/4$, but other workers are adamant that they find high EL quantum efficiencies consistent with a singlet:triplet formation ratio of about 1:1, implying $\sigma_S \approx 3\sigma_T$. To determine singlet:triplet formation ratios directly, rather than inferring them from EL to PL efficiencies, a systematic magnetic resonance

study on a number of organic semiconductors with band gaps in the visible range found that $\sigma_S/\sigma_T$ was indeed generally larger than 1, and between 2 and 5 for different materials. $\sigma_S/\sigma_T \approx 2$ to 5 corresponds to $\eta_{EL}$ of between $\sim 0.4\eta_{PL}$ and $\sim 0.6\eta_{PL}$ instead of $0.25\eta_{PL}$. Further work on an oligomer series has shown that $\sigma_S/\sigma_T$ increases with conjugation length, which implies larger $\sigma_S/\sigma_T$ for polymeric than for low molecular weight organic semiconductors. The marked violation of the naive 'one singlet to three triplets' rule for polymers (but not low molecular weight materials) may be explained as being the result of the relatively long quantum coherence in a polymeric organic semiconductor.

*Electrophosphorescence*

As alternative to the enhanced singlet formation cross section in polymers, the low molecular weight OLED community has developed the concept of harvesting triplets for light emission by using phosphorescence. In a typical electrophosphorescent device, a wide band gap host semiconductor is doped with a small percentage of a phosphorescent emitter. The excitation is transferred from the host to the guest via exciton energy transfer. Forrest and co-workers at Princeton have developed a range of green, yellow, orange and red organoiridium complexes, which are exemplified by the particularly efficient red phosphor $btp_2Ir(acac)$ (see the appendix). When doped into a wide band gap host, electrophosphorescence with better than 80% internal quantum efficiency and 60 lm $W^{-1}$ is observed.[4] Using pure $btp_2Ir(acac)$ without a host matrix had resulted in less efficient devices. In particular, electrophosphorescence is an attractive approach in the red. Due to the response characteristics of the human eye, red dyes must show very narrow emission peaks, otherwise colour purity will be compromised. Iridium-based phosphors display considerably narrower emission bands than typical fluorescent dyes, and are therefore particularly useful as red emitters. These phosphors also display relatively short triplet lifetimes (4 μs), thus avoiding problems associated with triplet–triplet annihilation at high brightness, which had been encountered with longer-lifetime phosphors. However, electrophosphorescence is ambitious for blue emission due to the need for a high band gap host semiconductor.

*Organolanthanides*

Another approach to triplet harvesting is represented by the organolanthanide dyes. Organolanthanides are somewhat similar to organometallic phosphors, but the central metal atom is a lanthanide such as europium (Eu) or terbium (Tb). The red dye ADS053RE is a typical example. Organolanthanides owe their properties to the unique electronic structure of the lanthanides (or rare earth metals), reflected by their positioning in the periodic table. In a dye such as ADS053RE the organic ligand can absorb light (typically in the blue or near UV), or can be excited electrically. The exciton is then passed to the central lanthanide and excites an electron of the lanthanide 4f shell; notably this works for singlet and triplet excitons. The intramolecular excitation

[4] Luminous efficiency is measured in lm $W^{-1}$ and is a measure of the light obtained for a given power input. For comparison, a typical incandescent light bulb has a luminous efficiency of typically less than 20 lm $W^{-1}$.

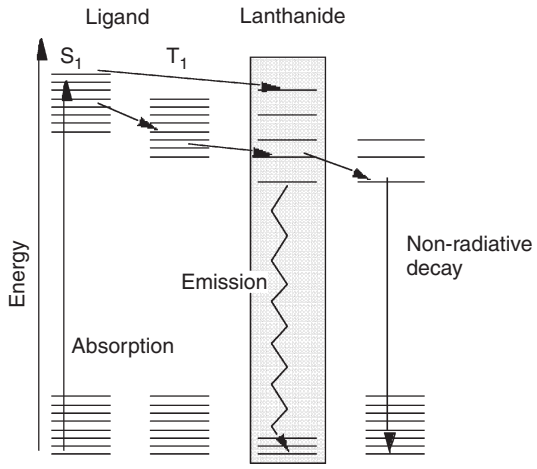


**Figure 6.18** An excitation migrates through the molecular (ligand) and atomic (lanthanide) levels in an organolanthanide

transfer is shown schematically in Figure 6.18. Note that the observed emission comes from the radiative decay of the excited 4f state; it is an atomic transition, *not* a molecular transition. This is the marked difference between organolanthanides and conventional organometallic phosphors. Due to the localized and isolated nature of the excited state, organolanthanides do not suffer from triplet–triplet annihilation. Efficiencies well in excess of 25% can be achieved. Since emission comes from an atomic transition, the bands are extremely narrow (FWHM $\approx$ 10 nm), resulting in very pure colours (green from terbium, red from europium).

There are two major drawbacks for organolanthanide applications. Firstly, for electrical excitation, carriers have to be injected into a rather large band gap material (deep blue or near UV) even if the emitted light is red. Larger band gaps generally make good, well-balanced carrier injection harder and lead to reduced power efficiencies and higher onset voltages. Also, as in all transfer-based concepts, the generation of blue light is somewhat problematic. Secondly, the bonding between a lanthanide and an organic shell has a considerable ionic (as opposed to covalent) character. The organic shell acquires a partial negative charge, the lanthanide a partial positive charge. When an electron is injected to the ligand, it becomes rather unstable against degradation. Consequently, until now, even for encapsulated organolanthanide devices, device lifetimes have been poor.

### *Conjugated dendrimers*

Another recent approach to improve the efficiency of light-emitting devices is the use of dendrons with a conjugated core surrounded by non-conjugated dendrimers. A schematic representation of the dendron concept is given in Figure 6.19. The conjugated core of the dendrimer can be either fluorescent or phosphorescent. The dendron concept seeks to combine the advantages of conjugated polymers and low molecular weight materials. Dendrimers can be processed from solution and form films in a manner

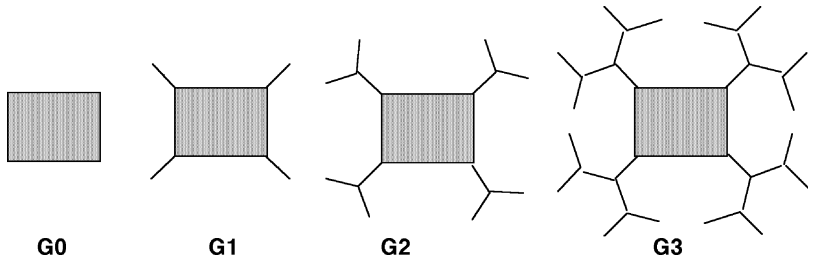


**Figure 6.19** Schematic representation of zeroth- to third-generation conjugated dendrimers. Shaded: conjugated core. Thin lines: dendronic side groups (non-conjugated)

similar to polymers. However, due to the dendronic side groups, individual chromophores are shielded from each other. This avoids some of the problems encountered when conjugated polymers are being used; due to interchain interactions such as aggregation and excimer formation, quantum efficiency may be reduced, and excimer emission may compromise colour purity. The major drawback of the dendrimer approach is the much reduced charge carrier mobility due to the increasing separation between conjugated units. The mobility $\mu$ scales with the separation between conjugated groups, $D$, with a characteristic length $R_0$ according to $\mu \propto D^2 \exp(-D/R_0)$.

A group at St Andrews University has studied dendrimers with a core consisting of three distyrylbenzene groups grouped around a central nitrogen, and dendrimeric side groups consisting of meta-linked vinylene phenylene groups, up to third generation. OLEDs made from higher-generation dendrimers displayed narrow EL spectra that approached the solution PL spectra of the conjugated core, and quantum efficiencies rose steeply with dendrimer generation. This is the result of a successful isolation of the emissive core groups from each other. Carrier injection was not affected by dendrimer generation, but the carrier mobility decreased dramatically. For second- and third-generation dendrimers, which did display narrow spectra and improved efficiency, the mobility was of the order of only $10^{-8}\,\mathrm{cm^2V^{-1}s^{-1}}$.

### *Light outcoupling*

After the efficient electrical generation of a photon, it must still leave the device to be observed by the viewer of the display. Practically, this outcoupling is often very inefficient, with often only 1 in 8 photons leaving the device. In other words, the *external quantum efficiency* $\eta_{\mathrm{ext}}$ is smaller than the internal quantum efficiency $\eta_{\mathrm{int}}$. The main loss mechanism here is in-plane waveguiding. To solve this problem, devices have been designed that suppress waveguiding. With a photoresist-based technique, the St Andrews group manufactured a corrugated anode that scatters light out of in-plane modes, hence, out of the device and towards the observer. In this way, $\eta_{\mathrm{ext}}$ was improved twofold. A more sophisticated approach for improved outcoupling is to establish a resonant vertical cavity mode in a device. Such cavities have spectrally narrow modes and a strong directional emission characteristic. Thus, spectrally pure colours can be generated even from broadband emitters. The principle of EL from resonant cavities has been established, but device manufacture is difficult due to the need to incorporate a dielectric mirror into the device architecture. Resonant cavities have proven a powerful tool for the

investigation of fundamental phenomena in quantum optics of organic semiconductors (strong coupling), but for practical devices probably will not be cost-efficient. They may, however, play an important role in future developments of organic injection lasers.

As a concluding remark, a single OLED device does not constitute a display that can communicate information, just as a single OFET does not represent a useful circuit. Consequently, device engineering issues are as prominent for OLED research as they are for OFETs, or even more so. Depending on the application, we may wish to have small or large, high-resolution, full-colour displays. This can only be achieved in pixellated displays, where individual pixels can be addressed independently. Currently, both *passive matrix* and *active matrix* displays are being developed.

## 6.2.4 Organic photovoltaics

The basic mechanism of photovoltaics is the reverse of electroluminescence. A solar photon is absorbed in a semiconductor, thus producing an exciton that has to be separated into electron and hole polarons, which migrate to opposite metal electrodes and discharge via an external load circuit, rather than recombining instantly under their mutual attraction. Obviously this exciton separation requires an internal field in the device that overcomes the electron–hole Coulomb attraction.

### 6.2.4.1 Basics of photovoltaic devices

Figure 6.20 shows the principle of a conventional (inorganic) photovoltaic device. A thin, semi-transparent layer of (in this case) a p-doped inorganic semiconductor is prepared on top of a thicker, n-doped layer. At the interface between the p layer and the n layer, a rectifying pn junction is formed. This results in the formation of a *depletion layer* with very few charge carriers, hence high resistivity, and a strong internal field. An exciton created by photon absorption near the pn junction may be torn apart by this field, and carriers will prefer to recombine via the external load $R$ if its resistance is smaller than that of the depletion layer. Figure 6.21 illustrates the $I/V$ characteristics of a rectifying junction in the dark and under illumination. $V$ is taken positive if it points from p to n (forward bias), and negative otherwise. Under illumination, if the p and n

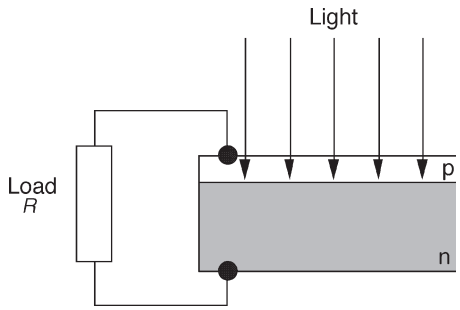


**Figure 6.20** A photovoltaic diode based on inorganic semiconductors

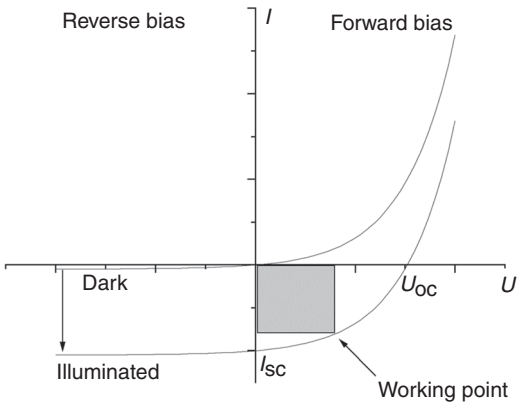


**Figure 6.21** Characteristics of pn junctions with and without illumination

terminals are shorted ($R = 0$), then even at $V = 0$ a current will flow due to photo-generated carriers, and in the opposite direction as a current under forward bias. Under illumination the $I(V)$ characteristic will be moved downwards by this *short-circuit current*, $I_{SC}$.

$I_{SC}$ is the maximum current the photovoltaic cell can deliver, and it will depend, among other factors, on the intensity of illumination. If the p and n terminals are unconnected ($R = \infty$), no current flows ($I = 0$) and the potential difference (voltage) between them will approach the intercept of the illuminated $I(V)$ characteristic with $I = 0$: the *open-circuit voltage* $V_{OC}$. $V_{OC}$ is the highest voltage that the photovoltaic cell can deliver. Within the lower quadrant of the I/$V$ diagram, between $I_{SC}$ and $V_{OC}$, the photovoltaic device can provide electrical power $P = VI$ to an external load. However, at $I_{SC}$, we have $V = 0$ hence $P = 0$, and at $V_{OC}$ we have $I = 0$ hence $P = 0$. To draw power from a photovoltaic cell, we have to sacrifice some bias and operate the cell at a working point $0 < V < V_{OC}$. The power drawn at $V$ can be represented as the area of a rectangle, which is shown shaded. At one particular $V_{max} < V_{OC}$, this rectangle will have maximum area; at this voltage the power delivered by the cell is maximised. The *fill factor* (FF) is defined as

$$\mathrm{FF} = \frac{P_{max}}{I_{SC} V_{OC}}, \tag{6.14}$$

which is often expressed as a percentage. FF is one of the most important characteristics of a photovoltaic cell, and large values of FF are obviously desirable. The efficiency of a photovoltaic cell is quantified by the *external quantum efficiency* (the number of carriers generated divided by the number of photons absorbed) and *power efficiency* $\eta_p$:

$$\eta_p = \frac{P_{out}}{P_{in}} = \left(\frac{I_{SC} V_{OC}}{LA}\right)\mathrm{FF}, \tag{6.15}$$

where $L$ is the light intensity and $A$ is the device area.

The key challenge in producing efficient solar cells is to harvest as many as possible of the incoming photons. This is made difficult by the fact that only excitons created near the pn interface, or more precisely within one exciton diffusion radius (~5 nm) of the interface, can possibly be separated into carriers. An exciton produced further away from the interface will recombine, maybe under fluorescence, but will not provide a current. Since typical absorption coefficients of inorganic semiconductors imply light penetration depths of order 100 nm even at maximum absorption, only a small fraction can generate excitons within the region of interest.

Early organic photovoltaic devices closely mimicked the architecture of inorganic heterojunction devices. Since organic semiconductors are intrinsically p- or n-type semiconducting without doping, no internal field develops at a heterojunction. Instead, this has to be established by the use of metals with unlike work functions. However, these devices suffer from the same problem as their inorganic counterparts; namely, most excitons are created too far away from the junction for harvesting.

#### 6.2.4.2 Organic bulk heterojunction diodes

The possibility to process organic semiconductors from solution is an asset that has been used to overcome the problem of short diffusion length. In the so-called *bulk heterojunction* photovoltaic devices, the electron donor and electron acceptor are spun from the same solution.

Typically, two unlike polymers, A and B, will not mix. A and B may share a common solvent and therefore may mix in solution, but in the solid state they will tend to separate into A and B islands. This incompatibility is a well-understood phenomenon for polymers in general, and has been the subject of much work in polymer physics. However, in the solid state at room temperature, conjugated polymers will typically be in a glassy state that does not allow for large-scale molecular rearrangements. How far phase separation will proceed during film preparation will therefore depend on the kinetics of the film formation process as compared to the kinetics of the phase separation process. In a fast film formation process such as spin-casting, phase separation may be arrested at an early stage, leading to a very fine texture, with A-rich and B-rich domain sizes of 100 nm or smaller. If both blend components are present in substantial amounts, this can lead to a *bicontinuous* structure, in which both components are *percolated*; that is, for each component, there is a path from the macroscopic faces of either side of the sample to the other which only consists of material of one component. Assuming that A and B are two semiconducting polymers, with A being an electron acceptor/transporter, and B an electron donor/hole transporter, then there is a conductive path for both electrons and holes through the whole film to reach their respective electrodes. This means that electrons and holes can be collected at opposite electrodes, in the same way as in discrete layer photovoltaic devices, thus fulfilling a necessary condition for photovoltaic applications. In the field of organic photovoltaics such a structure is sometimes called an *interpenetrating network* (not to be confused with a bicontinuous polymer mixture in which at least one of the components is cross-linked). Note that in a photoconductor system such as PVK/TNF, only holes have significant mobility while electrons are stuck. From a PVK/TNF blend, no photocurrent can be extracted, as the electrons left behind would rapidly build up a space charge field which would cancel any built-in field.

In a finely dispersed structure, the A–B interfacial area is much enhanced compared to discrete layer devices. Each A–B interface may act as a heterojunction to separate excitons into electrons and holes, so the entire layer represents a bulk heterojunction. When the length scale of the phase-separated structure is of the same order as an exciton diffusion length, then the bulk heterojunction approach will enable the separation of many more excitons than a discrete layer architecture. This is a key advantage of organic photovoltaics over inorganic photovoltaics.

A number of such bulk heterojunction photovoltaic devices have been reported in the literature. For example, a system based on PPV derivatives (MEH-PPV as hole transporter and CN-PPV as electron transporter) has achieved a rectification ratio of 1000 at $\pm 3.5\,\mathrm{V}$, $U_{OC}$ of 0.6 V and quantum efficiencies of up to 6%. A similar approach was based on MEH-PPV with a solubilized fullerene derivative, using a very similar material combination as had been studied for discrete layer devices. Note how the progress in materials chemistry that has made soluble $C_{60}$ derivatives available has enabled the realization of a new device concept. In that work, optimum performance was found at rather high fullerene load (80%), indicating that percolation is usually easier to achieve for a polymeric component than for a non-polymeric component. Quantum efficiencies approaching 3% have been reported. Devices where both components were fluorene copolymers have also been demonstrated. An interesting and novel approach is the use of electron-transporting low molecular weight materials that can crystallize after film preparation in a matrix of a polymeric hole transporter. In these systems the thermally activated growth of relatively large electron-transporting crystals with high electron mobilities within a hole-transporting matrix improves quantum efficiencies to up to 10%.

To comment on the remaining problems of organic photovoltaics, lifetime issues are important as always: in particular, the presence of oxygen leads to problems with long-term efficiency, similar to those encountered in OLEDs. Another crucial point is that the systems investigated so far are not very well suited to harvesting solar photons. Absorption and photocurrent action spectra of the studied materials typically peak in the mid-visible range, not at 1.4 eV in the near-infrared band, where the sun emits most photons per unit wavelength interval. This lack of suitable material represents a challenge to materials chemistry.

## 6.3 CARBON NANOTUBES

### 6.3.1 Structure

Shortly after the discovery of buckminsterfullerene in 1990, a related form of carbon was discovered, the carbon nanotube (CNT). CNTs consist of a graphene sheet which has been rolled up into a cylinder. The tube is energetically stable relative to the unrolled sheet because the unrolled sheet has a row of dangling bonds at its edges. For the same reason, CNTs are usually found to have hemispherical caps at one or both ends, made up of carbon hexagons and pentagons, such that the tube is a completely closed surface with no incomplete bonds at all. CNTs have an extremely high aspect ratio; a single-walled tube is typically 1–20 nm in diameter, but can be up to 100 mm in length. Multiwall nanotubes also exist and consist of several concentric carbon cylinders. Figures 6.22 and 6.23 show examples of single-wall and multiwall CNTs, respectively.

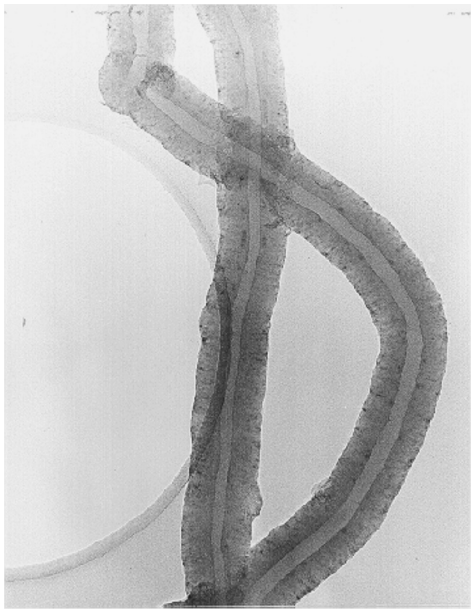

**Figure 6.22** TEM image of single-wall nanotubes. The diameter of each tube is approximately 3 nm. Image courtesy of R. Brydson, Institute of Materials Research, University of Leeds

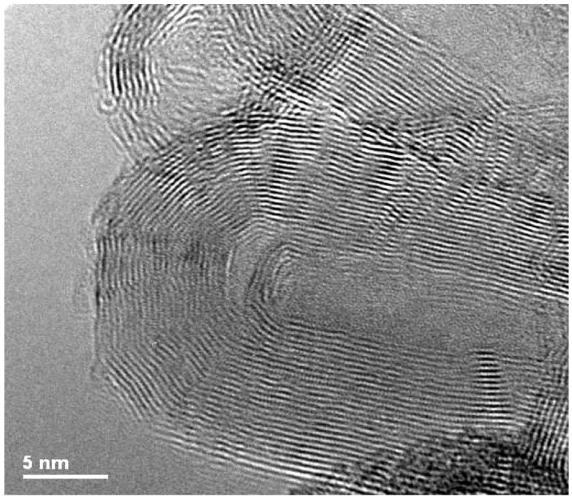


**Figure 6.23** TEM image of multiwall nanotubes. Image courtesy of Z. Aslam, X. Li, B. Rand and R. Brydson, Institute of Materials Research, University of Leeds

Theoretically, there exist an infinite number of permutations of tube structure, depending on how the two opposite sides of a graphene sheet are joined together to form the nanotube. There are two high-symmetry configurations which are *non-chiral*: the so-called *armchair* and *zigzag* tubes. In an armchair tube, the tube axis is perpendicular

to a line of C–C bonds in the graphene sheet, such that a thin ring cut from the tube will show a pattern of six-membered carbon hexagons joined to each other, vertex to vertex, by a C–C bond (Figure 6.24(a)). In a zigzag tube, the tube axis is parallel to a line of C–C bonds, such that a thin section cut from the tube shows a complete ring of carbon hexagons joined side to side as in Figure 6.24(b). All other tube configurations are *chiral*, with the tube axis offset relative to the two above cases, such that the chains of carbon hexagons can be traced in a spiral along the length of the tube. This is expressed mathematically by the *chiral vector*

$$\mathbf{C}_h = m\mathbf{a}_1 + n\mathbf{a}_2, \tag{6.16}$$

where $\mathbf{a}_1$ and $\mathbf{a}_2$ are unit vectors of the graphene sheet as shown in Figure 6.25. The chiral vector gives the direction normal to the tube axis on the graphene sheet. Thus, armchair tubes are all represented by chiral vectors with $m = n$, whereas zigzag tubes all have $n = 0$. The chiral vector is often abbreviated to $\mathbf{C}_h = (m, n)$.

The circumference of a zigzag tube $(m, 0)$ is thus given by $m|\mathbf{a}_1| = ma_C\sqrt{3}$ where the C–C bond length $a_C = 0.142\,\text{nm}$. Although CNTs can be formed with a wide range of

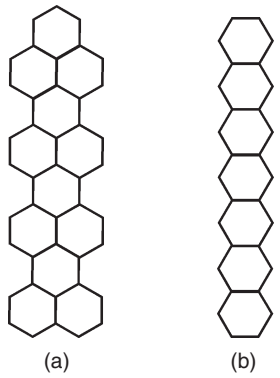


**Figure 6.24** Strips cut from the circumference of (a) an armchair nanotube and (b) a zigzag nanotube, showing the C–C bonds

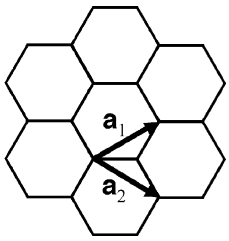


**Figure 6.25** Portion of a graphene plane showing the unit vectors $\mathbf{a}_1$ and $\mathbf{a}_2$

diameters, the minimum tube diameter is governed by the structure of the endcap, since the smallest stable cap is half a $C_{60}$ molecule.

### 6.3.2 Synthesis

The main synthesis methods for CNTs are laser ablation, arc discharge and CVD. In laser ablation, a graphite target is heated to 1200 °C in an argon atmosphere. Carbon is then evaporated from the target by a pulsed laser beam, and is collected on a cooled copper surface. The graphite target also contains small quantities of nickel and/or cobalt, which are also evaporated and deposited onto the copper surface; these act as catalysts for nucleation of the nanotubes. This method produces relatively wide (up to ~20 nm in diameter) and long (up to ~100 mm) nanotubes. The tubes often form in bundles or twisted ropes with a remarkably uniform distribution of diameters. However, the tangled nature of these bundles makes extraction and application of individual tubes very difficult. Tube growth is believed to occur via a *scooter* mechanism, in which a single catalyst atom travels, or scoots, around the end of an open tube, absorbing carbon from the argon atmosphere, and feeding this into the graphene sheet. Tube growth is terminated when the open end becomes saturated with catalyst atoms, at which point these detach from the tube, allowing a fullerene cap to form.

In the arc discharge method, a DC bias of 20–30 V is applied between two carbon electrodes in a helium atmosphere. Carbon atoms are ejected from the anode, and accumulate in the form of nanotubes on the cathode. The electrodes are typically 5–20 mm in diameter. As with laser evaporation, the anode includes small quantities of nickel, cobalt or iron, which are also deposited onto the cathode to act as a catalyst. Arc discharges tend to produce narrower and shorter tubes than those obtained from laser ablation (up to ~5 nm in diameter and around 1 mm long). Like laser ablation, arc discharges tend to produce bundles of nanotubes.

CVD synthesis of nanotubes involves decomposition of small hydrocarbon molecules (methane, ethene or acetylene) at temperatures between 500 and 1100 °C. The carbon atoms thus released are collected on a cooled substrate, which is pretreated with one of the above catalysts. CVD has the advantage that evaporation from a solid source is not involved, and promises to be the most amenable method for scaling up to large-scale production. Numerous variations on the CVD synthesis route have been explored, including PECVD for growth of well-aligned tubes (see below), and templated growth using porous silicon or lithographically defined arrays of catalyst particles.

In general, single-wall nanotubes cannot be grown in the absence of a catalyst. This implies that the catalyst atoms are essential in preventing the energetically favourable closure of the carbon cage by a process such as the scooting model described above. Multiwall nanotubes are better able to remain open-ended, as the exposed end of the concentric cylindrical structure is stabilized by extra carbon atoms which form bonds between adjacent graphene layers. These bonds can break and reform as the edge continues to grow. Single-wall nanotubes may also grow from the base upwards. In this model, nucleation on a catalyst particle produces a curved graphene sheet, which quickly forms a closed cap but remains open at its base. The open perimeter of the tube

is continually fed by carbon atoms adsorbed onto the catalyst from the reaction chamber, and these extend the tube from the bottom upwards.

### 6.3.3 Electronic properties

The electronic properties of CNTs are closely related to those of two-dimensional graphite. A single graphene sheet is a two-dimensional conductor that has energy bands which are degenerate at the Brillouin zone boundary, therefore it exhibits metallic behaviour. When a graphene sheet is rolled to form a CNT, free electronic motion is allowed only along the tube axis; only discrete electronic states can be supported around the circumference of the tube. CNTs are therefore one-dimensional conductors (or quantum wires), and they can behave as metals or semiconductors, depending on their exact structure. All armchair tubes are metallic, and their energy bands can be obtained from the dispersion relation for a graphene sheet:

$$E(k_x, k_y) = \pm\Delta\left\{1 \pm 4\cos\left(\frac{\sqrt{3}k_x a}{2}\right)\cos\left(\frac{k_y a}{2}\right) + 4\cos^2\left(\frac{k_y a}{2}\right)\right\}^{1/2}, \tag{6.17}$$

where the lattice constant $a = |\mathbf{a}_1|$ and the energy parameter $\Delta = 3.033\,\text{eV}$, by imposing the circumferential confinement relation

$$k_x = \frac{2\pi p}{\sqrt{3}am} \qquad (p = 1, \ldots, 2m) \tag{6.18}$$

on the wavevector $k_x$. Note here that $k_x$ and $k_y$ represent wavevector components in the two-dimensional reciprocal lattice of graphene which, like the real space lattice, also has hexagonal symmetry with the $k_y$ and $k_x$ axes directed parallel and perpendicular to a hexagon side, respectively.

For zigzag nanotubes, the appropriate confinement condition is

$$k_y = \frac{2\pi p}{am} \qquad (p = 1, \ldots, 2m). \tag{6.19}$$

By substituting this condition into Equation (6.17), it can be seen that there is zero energy gap (metallic behaviour) at $k_x = 0$ whenever $m$ is a multiple of three. In general, an $(m, n)$ nanotube will be metallic if $m - n$ is a multiple of three. For all other tubes, an energy gap persists throughout the Brillouin zone, and the size of this gap varies inversely with the tube diameter. Thus, in a random collection of nanotube structures, one-third of the tubes will be metallic and two-thirds will be semiconducting.

The confinement conditions given by Equations (6.18) and (6.19) lead to a large number of energy subbands in the energy band structure. Figures 6.26 and 6.27 show energy bands for armchair and zigzag tubes, respectively. The energy bands in both cases have zero gradient at the zone centre which, for a one-dimensional conductor, gives rise to Van Hove singularities in the density of states, analogous to the case of

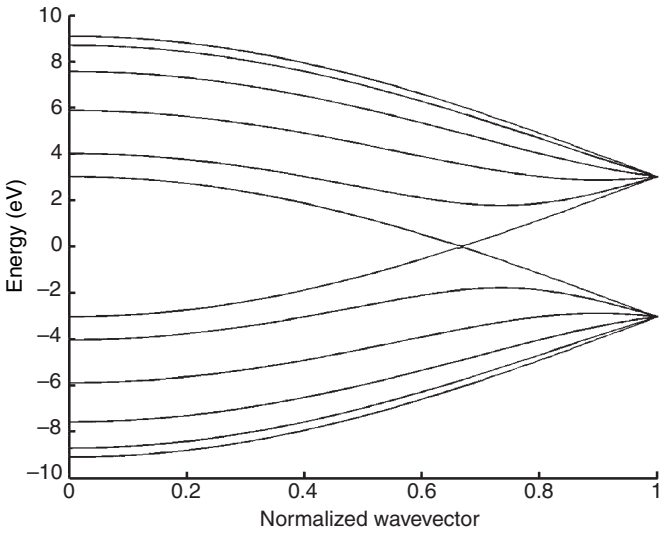


**Figure 6.26** Electronic band structure for a (5, 5) armchair nanotube. The wavevector is normalized to the position of the Brillouin zone boundary, $k_y = p/a$

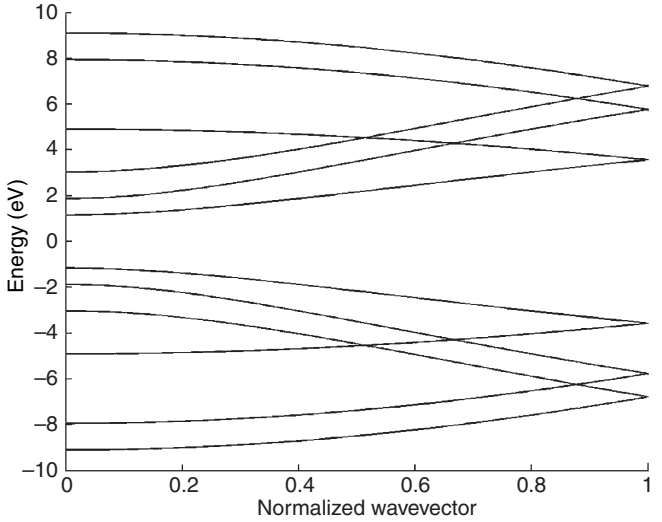


**Figure 6.27** Electronic band structure for a (5, 0) zigzag nanotube. The wavevector is normalized to the position of the Brillouin boundary, $k_x = p/(a\sqrt{3})$

semiconductor quantum wires (Chapter 3). The armchair nanotube has two crossing bands, resulting in metallic behaviour, whereas the (5, 0) zigzag tube shown in Figure 6.27 has a clear band gap, hence it is a semiconductor. Figure 6.28 shows the band structure for a (6, 0) zigzag tube; this satisfies the condition described above for metallic behaviour, and the band gap reduces to zero at the Brillouin zone centre.

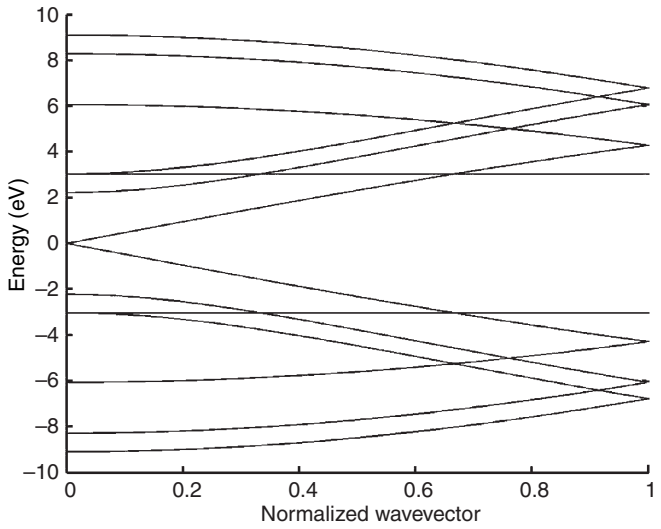


**Figure 6.28** Electronic band structure for a (6, 0) zigzag nanotube. The wavevector normalization is as for Figure 6.26

Since the electronic states are confined in the directions perpendicular to the tube axis, electron momentum is only defined in the axial direction, therefore scattering (by phonons or impurities) is constrained to be purely in the forward direction (zero scattering angle) or purely in the reverse direction (backscattering or 180° scattering angle). This restriction greatly affects the transport properties of CNTs relative to bulk materials. At low temperatures, transport is ballistic, and the conductance becomes dependent on the length of the tube. For metallic nanotubes, the tube resistance is generally much less than the contact resistances between the tube and the connecting leads. In this configuration the tube exhibits Coulomb blockade behaviour (Section 3.6.4), with electron transfer into the tube suppressed by the presence of a single electron. The $I/V$ curve contains steps, corresponding to an abrupt increase in current every time the bias is raised sufficiently to match the electrostatic charging energy required to place another electron on the tube. This behaviour persists up to temperatures of around 20 K in isolated single-wall nanotubes.

CNT analogues of electronic metal–semiconductor, semiconductor–semiconductor or metal–metal junctions can be formed by joining two tubes of different chiralities. The transition between the two tubes is accomplished by defects in the hexagonal carbon lattice, so a kink usually occurs at the junction.

## 6.3.4 Vibrational properties

Just as the electronic band structure of CNTs is related to that of a two-dimensional graphene sheet, so too are the vibrational modes or phonon band structure. Although extended vibrational waves can exist parallel to the tube axis, only certain mode

configurations can be supported around the circumference of the tube, giving rise to a large number of closely spaced phonon subbands. The exact definition of the unit cell of a CNT depends on the chirality of the tube. In general, if the tube has a unit cell which contains $2N$ carbon atoms, then there will be $6N$ phonon modes. Four of these modes are acoustic, leaving $6N-4$ optical modes. Of the four acoustic modes, there are two transverse modes, in which the carbon atoms are displaced in the $x$ and $y$ directions, respectively, relative to the tube axis ($z$), and a longitudinal mode in which the displacement is parallel to the tube axis. The fourth acoustic mode is a twisting mode, so called because it involves a twisting motion of the tube about its axis, with the atomic displacements preserving the cylindrical topology. The optical modes include a radial breathing mode, in which all the atoms in a circle around the tube move in and out, in phase. This mode can be readily detected using Raman spectroscopy, and provides quite a sensitive measure of the tube diameter. Related to the radial breathing mode are a whole family of optical modes characterized by displacement waves around the tube circumference which have 1,2,3, ... nodes.

The phonon modes of CNTs give the dominant contribution to their thermal properties in the temperature range $\sim 10-400$ K. Molecular dynamics simulations of phonon modes in individual CNTs have predicted thermal conductivities of up to $4 \times 10^4$ W m$^{-1}$K$^{-1}$, significantly greater than those of both diamond and in-plane graphite. Such predictions raised great hopes that CNTs could be used for thermal management (component cooling) applications. However, it appears that the theoretically predicted values are difficult to realize in practice. Measurements on individual multiwall CNTs have yielded room temperature thermal conductivities of $\sim 3000$ W m$^{-1}$K$^{-1}$, but in samples containing large numbers of tubes, where a thermal connection cannot be made directly to both ends of each tube, the thermal conductivities are much lower. The thermal conductivity for a single tube is highly anisotropic; large values only prevail parallel to the tube axis, and it appears that the interfaces between separate tubes present large thermal resistances.

### 6.3.5 Mechanical properties

One aspect of CNTs which has particularly captured the imagination of many is their remarkable mechanical strength; popular reviews often quote statements such as 'a hundred times the strength of steel at one sixth of the weight'. The strength of CNTs is directly related to the C=C bond, which is one of the strongest of all chemical bonds, and to the relatively small number of crystalline defects present in the tubes. Evaluation of the tensile strength and the Young's modulus of CNTs is obviously difficult, due to their small size, and a range of methods have been employed, including TEM monitoring of tube vibrations, AFM manipulation and computer simulation. The measured tensile strength (the maximum load before breaking) of CNTs is typically around 50 GPa, compared with a theoretical maximum of 150 GPa for a completely defect-free tube. The compressive strength is slightly higher still, with measured values of around 100 GPa. In comparison, the tensile strength of steel is 2 GPa. The measured Young's modulus of CNTs is approximately 1 TPa, with simulation predicting a maximum value of over 5 TPa. Again, these values are

considerably higher than for steel, which has a Young's modulus of 0.21 TPa. Under high tensile strain, dislocations form in which an adjacent pair of carbon hexagons distorts into a heptagon and joined pentagon. These 5/7 dislocations change the local chirality, hence the diameter of the tube. Multiple-wall CNTs show similar mechanical properties to single-wall tubes; however, it appears that normally only the outer tube can be coupled to the mechanical load, since the bonding between the different concentric layers is too weak to provide effective load transfer. Bundles of nanotubes show mechanical properties that are comparable, but somewhat weaker than those of single tubes, because of the difficulty of sharing the load equally between all the tubes. It is thought that twisting a bundle of tubes into a nanorope will increase mechanical strength by improving the mechanical coupling between the tubes.

Because of their high aspect ratio, CNTs are susceptible to buckling and bending when stress is applied perpendicular to the tube axis. However, unlike many materials, they are highly resilient to severe bending; rather than creating defects which crack the tube, the bending results in a rehybridization of the $sp^2$ bonds, a process which is reversible if the tube is straightened out again. Bending can be induced by AFM probing, and has been observed in TEM images. Collapse of the tube cross section has also been observed, resulting in flat carbon ribbons. Cross-sectional collapse is energetically more likely for large-diameter tubes (>3 nm).

## 6.3.6 Applications

### 6.3.6.1 Carbon nanotube transistors

In many respects, carbon nanotubes are extremely well suited for use as the conducting channel of a field effect transistor (FET). The high conductivity of CNTs gives high current handling and low power dissipation, while their strong charge confinement reduces the detrimental effects associated with reduction of transistor size – *short channel effects* – primarily, the loss of the ability of the gate contact to control charge flow between source and drain. Since CNTs are formed completely from covalent bonds, they do not suffer from electromigration effects under high-current drive, and since all the bonds in a CNT are properly connected, there are no exposed surfaces that require passivation. Consequently, there is no restriction on the choice of gate dielectric material: CNTs can be used with any one of a range of new high dielectric constant materials (high-*k* dielectrics) that are currently being investigated as an alternative to silicon dioxide. The conduction and valence bands in CNTs are symmetric, with both electrons and holes having the same effective mass; this means that CNT-based FETs are ideal, in principle, for complementary logic, since both n- and p-type transistors will operate at the same speed. Finally, the fact that semiconducting CNTs have a direct band gap raises the interesting possibility of integrated CNT-based optoelectronic systems.

A CNT FET can be formed by draping the nanotube between source and drain contacts as shown in Figure 6.29. A highly doped silicon layer underneath the CNT, and insulated from it by a thin oxide layer, acts as the gate contact of the FET. Without any intentional doping the CNT acts as a hole conductor, forming a

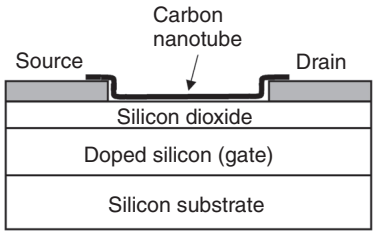


**Figure 6.29** Schematic diagram of a carbon nanotube FET

p-channel device; n-channel devices can be formed by doping the CNT with an element such as potassium. The interfaces between the CNT and the source and drain contacts (usually formed from aluminium) are Schottky contacts; i.e., there is a potential barrier between the two materials. The barrier height can be reduced by increasing the tube diameter, which reduces its band gap and effective mass. The Schottky barriers lead to other interesting properties; for example, following oxygen exposure and annealling, a p-channel CNT FET can be converted to an n-channel device, since the electronic properties of the Schottky barriers are altered by oxygen adsorption on the source and drain contacts.

Top-gated CNTs have been fabricated by positioning the tube between source and drain contacts on an $SiO_2$ surface as before, and then growing a thin covering layer of $SiO_2$ before depositing a metal or polysilicon gate layer. It is also possible to fabricate side-gated CNT FETs by depositing a gold stripe perpendicular to the nanotube. Gold does not adhere to the nanotube, and therefore the resultant structure has metal contacts on either side of the tube, but with each separated from it by a small gap. A similar effect can be obtained with chromium.

CNTs may also be used as the basis of chemically sensitive FETs for sensing applications. For example, detection of $NO_2$ by a CNT FET has been demonstrated; the $NO_2$ molecules are adsorbed by the nanotube, creating additional free holes, which increase the tube conductivity. Further work is needed to produce a sensor whose response is reversible on removing the reagent from the atmosphere.

#### 6.3.6.2 Field emission

Field emission – the electric field induced emission of electrons from a solid – is readily obtained in CNTs. Theoretically, the geometry of a CNT, comprising a long, thin cylinder terminated in a hemispherical cap, results in one of the highest attainable surface fields at its tip, relative to other attainable tip shapes. A CNT field emission device can then be made by applying a voltage between two electrodes, one of which is coated with an array of nanotubes.

An important commercial application of this property is in flat panel displays. Using transparent electrodes and an addressable array, pixels of field-emitting CNTs can be switched to excite red, green or blue phosphors and hence create a full-colour image. Compact (5″ diagonal) colour CNT displays have already been demonstrated, which

have very high brightness compared to alternative display technologies. The electrons emitted from CNTs can be accelerated to such an extent that X-rays, rather than visible light, can be emitted from a target, and CNTs have already been used commercially in cold cathode X-ray sources for lead detection.

In these initial applications of CNTs for field emission, the tubes were deposited in a random array on the electrode surface. The random orientation of the tubes gives an inherent screening of the resultant electric field, relative to the ideal scenario in which all tubes would be aligned perpendicular to the electrode plane. Alignment of the nanotube array can be attained by careful control of the growth conditions using a PECVD technique. The screening effect can also be reduced by control of the lateral tube–tube spacing; the optimum spacing is approximately $2l$, where $l$ is the average tube length, and this can be achieved by templated growth on isolated dots of a nickel catalyst. With such improvements in fabrication technology, other applications for field-emitting CNTs are under development, such as high-power microwave amplifiers and electron gun arrays for parallel electron beam lithography.

#### 6.3.6.3 Mechanical reinforcement

Individual CNTs have excellent mechanical properties. However, the exploitation of these properties in bulk materials is a major challenge. One important approach is the formation of composite materials in which a small percentage of CNTs are incorporated into a metal or polymer host. This method has already been demonstrated for polypropylene and aluminium, with a doubling in tensile strength observed in both cases. Theoretical predictions show that the tensile strength of steel could be increased by a factor of 3 by the addition of just 10% by weight of CNTs.

#### 6.3.6.4 Fuel cells

There has been great optimism that CNTs could be used as hydrogen storage vessels for application in non-fossil-fuel cells. Carbon is one of the most lightweight materials to remain solid at room temperature, and the graphene sheet presents a very high surface area to weight ratio. Graphite itself has not proved useful for hydrogen adsorption, since only a small proportion of the surface interacts with hydrogen molecules; however, it was envisaged that CNTs would have the added benefit of capillary forces which would draw hydrogen inside.

Simulations have shown that the adsorption of hydrogen by CNTs decreases rapidly with increasing temperature. A maximum storage capacity of 14% by weight is predicted at cryogenic temperatures and high pressures, based on the maximum number of covalent C–H bonds that can be formed inside the tube. This scenario is impractical since the hydrogen cannot be released unless the temperature is raised considerably. At room temperature, the predicted storage capacity drops to below 1% by weight. (As an indication of practical utility, the US Department of Energy has cited a value of 6.5% storage capacity as a minimum requirement for vehicular

applications.) Experimentally, much higher storage capacities (over 60% by weight) have been reported, but these have not proved reproducible. In some cases the high reported values appear to be a consequence of contamination or adsorption of other gases present in the system. To this end, further progress requires, among other things, improvements in the purification of CNTs. Another key issue is to devise a storage process that is not only reversible, but also provides useful capacity at convenient operating temperatures.

# APPENDIX: REFERENCE TABLE OF ORGANIC SEMICONDUCTORS

## Low molecular weight organic semiconductors

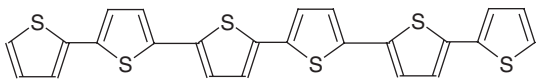


6T

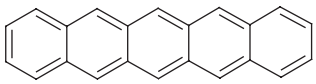

Pentacene

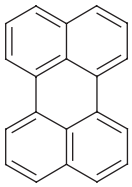

Perylene

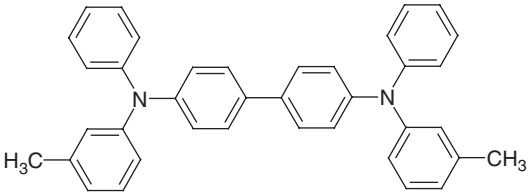


TPD

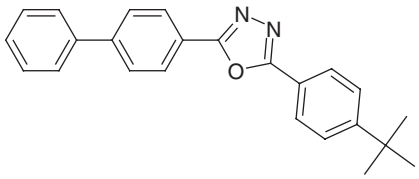


PBD

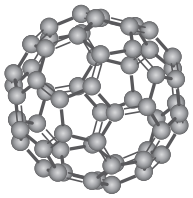

$C_{60}$

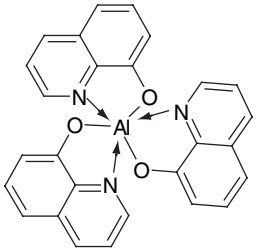


$Alq_3$

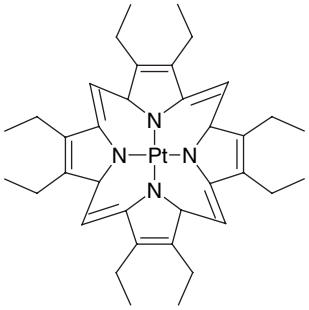


PtOEP

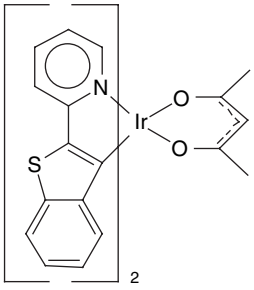


btpacac

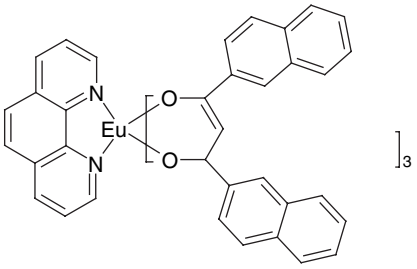


ADS053RE

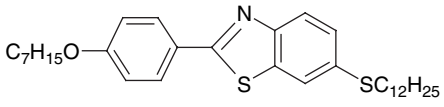


7O-PBT-S12

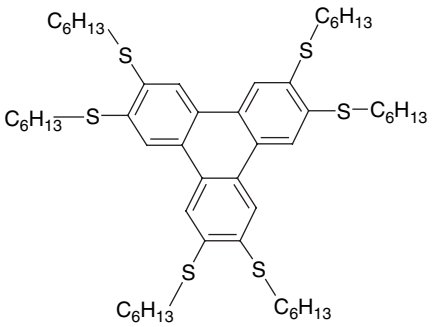


HHTT

Hexithiophene (6T), Pentacene, Perylene, and TPD (*N, N*′-bis-(*m*-tolyl)-*N, N*′diphenyl-1,1-biphenyl-4,4′-diamine) are hole-transporting and more or less strongly fluorescent organic semiconductors Perylene is more emissive, the others, less. 6T is one representative of the thiophene family of organic semiconductors, which are known for their fast hole mobilities and are often used in organic transistors. PBD (2-(biphenyl-4-yl)-5-(4-tert-butylphenyl)-1,3,4-oxadiazole) is an electron conductor. Both TPD and PBD have been used as carrier injection layers in multilayer device architectures. $C_{60}$ is a material with very high electron affinity, and $C_{60}$ derivatives have been used as electron acceptors in organic photovoltaic devices. However, electron transport in $C_{60}$ is very sensitive to even traces of oxygen, which limits its practical potential. $Alq_3$ (tris(8-quinolinolato)aluminum(III)) is an organometallic Al chelate complex with efficient green electroluminescence and remarkable stability. $Alq_3$ was used as the emissive material in the first double-layer organic light-emitting device. PtOEP is a red phosphorescent porphyrine derivative. The central Pt atom facilitates spin–orbit coupling that allows light emission from triplet excitons. $btp_2Ir(acac)$ (bis(2-(2′-benzothienyl)-pyridinato-*N,C*-3′) iridiumacetylacetonate) is a representative of a family of highly efficient phosphors that have been used successfully as triplet-harvesting emitters in efficient electrophosphorescent devices. ADS053 RE is a trade name for the red-emitting organolanthanide Tris(dinapthoylmethane)mono(phenanthroline)-europium(III). Organolanthanides transfer both singlet and triplet excitons to an excited atomic state of the central lanthanide, resulting in very narrow emission lines; i.e., spectrally pure colours (here the 612 nm red line of europium). 7O-PBT-S12 and HHTT are hole-transporting calamitic and discotic liquid crystals, respectively. Due to the stacking of conjugated cores in smectic (7O-PBT-S12) and some discotic (HHTT) liquid crystalline phases, both can display rather high charge carrier mobilities.

## Polymeric organic semiconductors

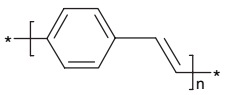

PPV

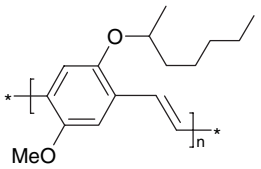


MEH-PPV

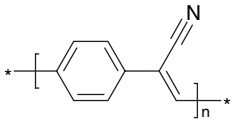


CN-PPV

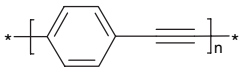

PPE

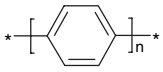

PPP

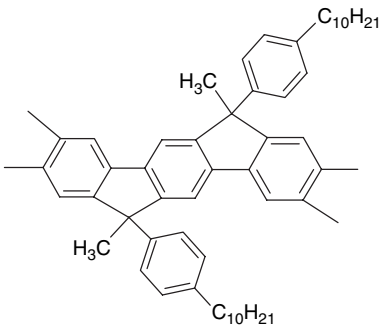


MeLPPP

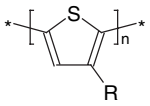


PAT

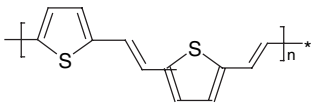


PTV

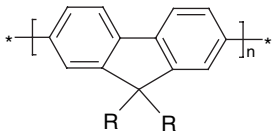


PF

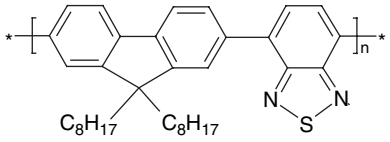


F8BT

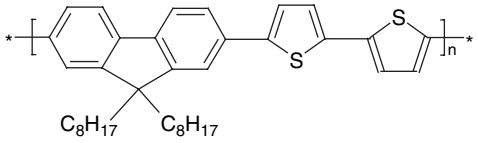


F8T2

Poly(*p*-phenylene vinylene) (PPV) played an outstanding role in the development of organic electroluminescence. MEH-PPV and Cyano-PPV (CN-PPV) are side chain substituted PPVs. Side chains promote solubility and can also change the band gap. Poly(phenylene ethynylene) (PPE) and poly(*p*-phenylene) (PPP) are variations on a similar theme. Methylated ladder-type PPP (MeLPPP) is similar to PPP, but with all backbone rings coplanar. PPVs, PPP, PPE and MeLPPP have been explored extensively in organic light-emitting devices. Poly(alkylated thiophene) (PAT) and poly(thienylene vinylene) (PTV) are less emissive, but have favourable properties in organic FETs. Polyfluorene (PF) is a blue emitter that has recently competed successfully with PPV as organic light-emitting material. Typically, PF is copolymerized rather than side chain substituted to modify its properties. F8BT is an electron transporter and efficient green emitter. F8T2 is a hole transporter that works well in transistors. PF, F8BT and F8T2 also display interesting liquid crystalline phases.

## 'Hybrid' materials

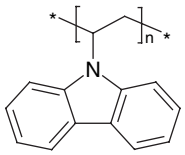


PVK

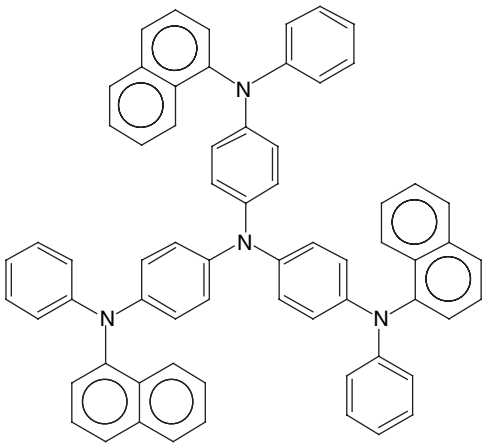

ST 638

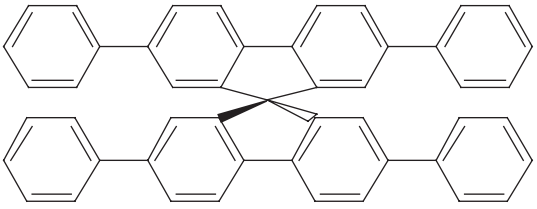

sQP

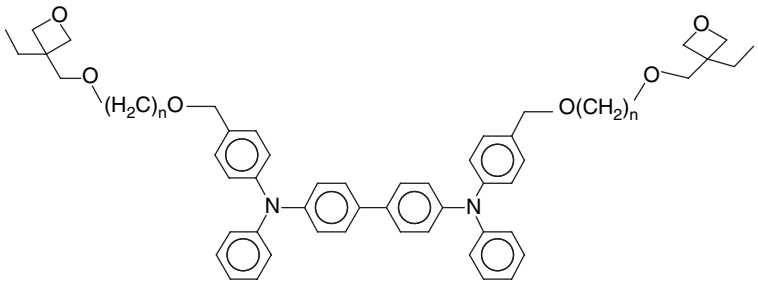


oxTPD

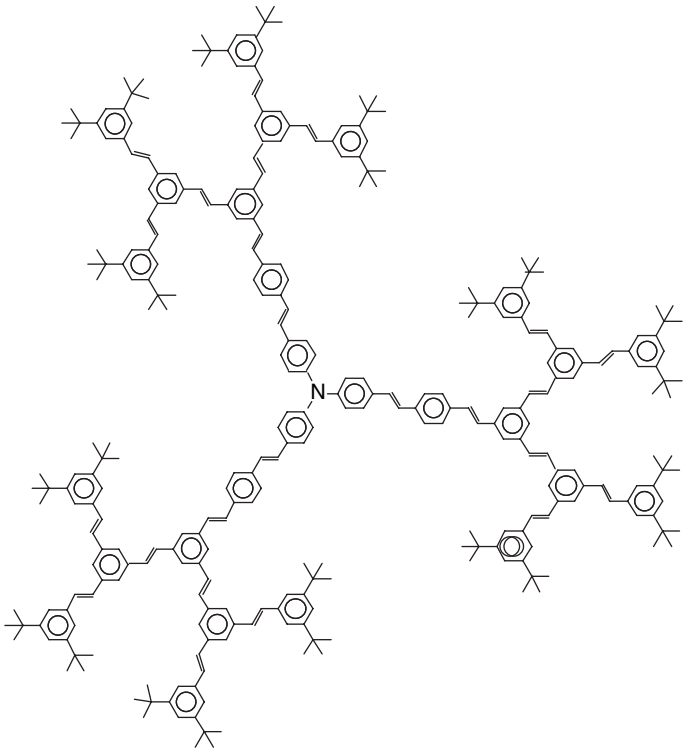


NDSB Dendron (G2)

Poly(vinyl carbazole) (PVK) is historically one of the first polymeric organic semiconductors. It is a polymeric material, with the film-forming and morphological properties typical of polymers. However, the semiconducting carbazole units dangle laterally from a non-conjugated backbone and are isolated from each other. The electronic properties of PVK are therefore very similar to those of low molecular weight carbazole. ST 638 is the trade name for 4,4′,4″-tris(*N*-(1-naphthyl)-*N*-phenyl-amino)-triphenylamine. This is low molecular weight material, but due to its sterically hindered 'starburst' architecture it has a very high glass transition temperature and typically does not crystallize when spin-cast from solution, but forms a glassy film, like many polymers. The glassy morphology has considerable advantages for device applications; a tendency to crystallize is a major problem with hole-transporting small molecules such as TPD. The same structural theme was employed for the design of electron-transporting starburst-type phenylquinoxalines (not shown here). Another structural theme that can be used to suppress crystallization in non-polymeric materials is the use of spiro links between two (or more) *p*-phenylene units, here exemplified by a spiro-linked pair of quaterphenyls (sQP). Note the cross-shaped three-dimensional architecture of spiro compounds that is difficult to sketch on paper. oxTPD is clearly a low molecular weight compound, but via the oxetane functions that are attached with flexible spacers it can be cross-linked in situ with the help of a suitable (photo)initiator. The result is a highly cross-linked, inert

hole-transporting film with no crystallisation tendency that has been used successfully in multiplayer devices. NDSB Dendron (G2) is a second-generation, nitrogen-cored distyryl benzene dendrimer. The core displays visible absorption and emission, the meta-linked dendronic side groups have a band gap in the UV, and for charge injection, transport and light emission they can be considered as inert.

## Synthetic metals

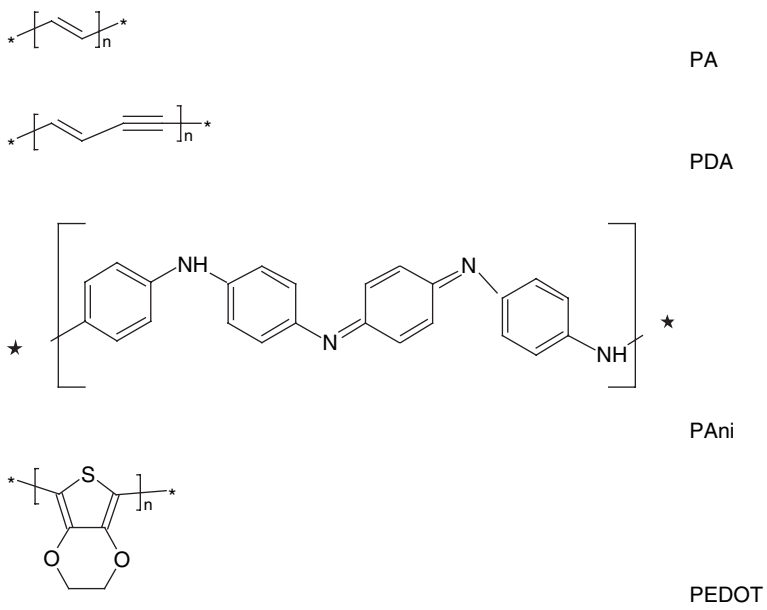


The distinction between organic semiconductors and synthetic metals is somewhat arbitrary, as the synthetic metals shown here are in the undoped state, when they display semiconducting rather than metallic or quasi-metallic properties. Metallic properties are induced by chemical doping with a substance that is either highly redox active, or an acid or a base. Poly(acetylene) (PA) is the classic example; the (chance) discovery that iodine-doped PA displays metallic conductivity was a milestone that earned the 2000 Nobel prize in chemistry. Poly(diacetylene) (PDA) has a widely tunable band gap if substituted with suitable side groups. Both PA and PDA are of historic, but no longer practical, interest. Poly(aniline) (PAni, here shown as emeraldine base) and poly (3,4-ethylenedioxythiophene) (PEDOT) are more modern developments. They are made metallic by acid rather than redox doping. Water-based PAni and PEDOT preparations are now commercially available. PEDOT that is acid-doped with poly(styrene sulfonic acid) (PSS), PEDOT/PSS, is now very popular in the OLED community to modify or replace the commonly used transparent ITO anodes.

# BIBLIOGRAPHY

## Books

An excellent text on the physics of solids is *Solid State Physics* by N. W. Ashcroft and N. D. Mermin, published by Holt, Rinehart and Winston, New York, 1977.

A good discussion of electronic transitions is given in *Physical Chemistry*, 5th edn, by P. W. Atkins, Oxford University Press, Oxford, 1994.

Much of interest, especially concerning space charge limited current, is contained in *Functional Organic and Polymeric Materials*, edited by T. H. Richardson and published by John Wiley & Sons, Ltd, Chichester, 2000.

Liquid crystalline polymers are discussed by A. M. Donald and A. H. Windle in their book *Liquid Crystalline Polymers*, Cambridge University Press, Cambridge, 1992.

## Review articles

Tuning the bandgap in organic semiconductors: A. Kraft, A. C. Grimsdale and A. B. Holmes, *Angew. Chem. Int. Ed.*, **37**, 403 (1998); D. N. Batchelder, *Contemp. Phys.* **29**, 3 (1988).

PEDOT/PSS: L. Groenendaal, F. Jonas, D. Freitag, H. Pielartzik and J. R. Reynolds, *Adv. Mater.* **12**, 481 (2000).

Synthetic metals: A. B. Kaiser, *Adv. Mater.* **13**, 928 (2001).